



THE UNIVERSITY *of* EDINBURGH

Edinburgh Research Explorer

## Protective role of chaperone-mediated autophagy against atherosclerosis

### Citation for published version:

Madrigal-Matute, J, de Bruijn, J, van Kuijk, K, Riascos-Bernal, DF, Diaz, A, Tasset, I, Martín-Segura, A, J.J. Gijbel, M, Sander, B, Kaushik, S, Biessen, EAL, Tiano, S, Bourdenx, M, J. Krause, G, McCracken, I, Baker, AH, Han, J, Sibinga, N, Bravo-Cordero, JJ, Macian, F, Singh, R, Rensen, PCN, Berbée, JFP, Pasterkamp, G, Sluimer, J & Cuervo, AM 2022, 'Protective role of chaperone-mediated autophagy against atherosclerosis', *Proceedings of the National Academy of Sciences*.  
<https://doi.org/10.1073/pnas.2121133119>

### Digital Object Identifier (DOI):

[10.1073/pnas.2121133119](https://doi.org/10.1073/pnas.2121133119)

### Link:

[Link to publication record in Edinburgh Research Explorer](#)

### Document Version:

Peer reviewed version

### Published In:

Proceedings of the National Academy of Sciences

### General rights

Copyright for the publications made accessible via the Edinburgh Research Explorer is retained by the author(s) and / or other copyright owners and it is a condition of accessing these publications that users recognise and abide by the legal requirements associated with these rights.

### Take down policy

The University of Edinburgh has made every reasonable effort to ensure that Edinburgh Research Explorer content complies with UK legislation. If you believe that the public display of this file breaches copyright please contact [openaccess@ed.ac.uk](mailto:openaccess@ed.ac.uk) providing details, and we will remove access to the work immediately and investigate your claim.



## Protective role of chaperone-mediated autophagy against atherosclerosis

Julio Madrigal-Matute<sup>a,b</sup>, Jenny de Bruijn<sup>c</sup>, Kim van Kuijk<sup>c</sup>, Dario F Riascos-Bernal<sup>d</sup>, Antonio Diaz<sup>a,b</sup>, Inmaculada Tasset<sup>a,b</sup>, Adrián Martín-Segura<sup>a,b</sup>, Marion J.J. Gijbel<sup>c,e</sup>, Bianca Sander<sup>c</sup>, Susmita Kaushik<sup>a,b</sup>, Erik A.L. Biessen<sup>c</sup>, Simoni Tiano<sup>a,b</sup>, Mathieu Bourdenx<sup>a,b</sup>, Gregory J. Krause<sup>a,b</sup>, Ian McCracken<sup>f</sup>, Andrew Baker<sup>f</sup>, Han Jin<sup>c</sup>, Nicholas Sibinga<sup>a,d</sup>, Jose Javier Bravo-Cordero<sup>g</sup>, Fernando Macian<sup>h</sup>, Rajat Singh<sup>a,b,d</sup>, Patrick C.N. Rensen<sup>i</sup>, Jimmy F.P. Berbéel<sup>j,2</sup>, Gerard Pasterkamp<sup>k</sup>, Judith C. Sluimer<sup>c,f,1,\*</sup>, Ana Maria Cuervo<sup>a,b,d,1,\*</sup>.

<sup>a</sup>Department of Development and Molecular Biology, <sup>b</sup>Institute for Aging Studies, Albert Einstein College of Medicine, 1300 Morris Park Avenue, Bronx, NY, 10461, USA. <sup>c</sup>Department of Pathology, Cardiovascular Research Institute Maastricht (CARIM), GROW-School for Oncology and Developmental Biology, Maastricht University Medical Center P. Debyelaan 25, 6229 HX, Maastricht, The Netherlands, <sup>d</sup>Department of Medicine Albert Einstein College of Medicine, 13300 Morris Park Avenue, Bronx, NY, 10461, USA, <sup>e</sup>Department of Medical Biochemistry, Experimental Vascular Biology, Amsterdam UMC, University of Amsterdam, Amsterdam, the Netherlands, <sup>f</sup>Centre for Cardiovascular Science, University of Edinburgh, Edinburgh, UK, <sup>g</sup>Department of Medicine, Division of Hematology and Medical Oncology, Icahn School of Medicine at Mount Sinai, New York 10029 NY, USA. <sup>h</sup>Department of Pathology, Albert Einstein College of Medicine, 13300 Morris Park Avenue, Bronx, NY, 10461, USA. <sup>i</sup>Department of Internal Medicine, Section Endocrinology Leiden University Medical Center, Leiden, The Netherlands, and Einthoven Laboratory for Experimental Vascular Medicine, Leiden University Medical Center, Leiden, The Netherlands. <sup>j</sup>Department of Experimental Cardiology Laboratory, Utrecht University Medical Center, Heidelberglaan 100, 3584 CX Utrecht, the Netherlands,

\* Co-corresponding

<sup>1</sup> Equal contribution to this work

<sup>2</sup>Deceased

Correspondence may be addressed to: Ana Maria Cuervo MD PhD, Albert Einstein College of Medicine, 1300 Morris Park Avenue, Bronx, NY 10461, USA. Phone: 718 30 2689 [ana-maria.cuervo@einsteinmed.edu](mailto:ana-maria.cuervo@einsteinmed.edu) and Judith Sluimer PhD, Maastricht University Medical Center, P

Debyeplein15, DEB15, 6229 HA Maastricht, Netherlands Phone: 31 43 387 7675  
[judith.sluiser@maastrichtuniversity.nl](mailto:judith.sluiser@maastrichtuniversity.nl)

**Author Contributions:** JMM designed and performed biochemical and image-based experiments, analyzed and interpreted the data, wrote the first draft and edited later versions of the manuscript; JdB, KvK, BS, DFR-B and MJJG performed histological staining and analysis of human and mouse arteries, analyzed and interpreted the data and contributed to editing of the manuscript; AD assisted with animal genotyping, diets and maintenance; IT generated and systemically characterized the LAMP-2A OE mice; AM-S and GJK assisted with the metabolic characterization of the mouse models and ITT analysis; ST assisted with sample collection and biochemical analysis; SK and RS assisted with viral delivery and mice treatments; JJB-C performed the two-photon and intravital imaging of KFERQ-Dendra aorta; FM performed immunological characterization; EALB and JCS coordinated the Paired Segment of Carotid Endarterectomy samples “MaasHPS” Biobank; MB performed the computational analysis; HJ and IMcC analyzed human plaque microarray and single cell sequencing data; PR and JB performed the cholesterol and TG profile; GP collected the prospective AtheroExpress Study Biobank with human carotid plaques; AMC and JCS coordinated the study, coordinated the autopsy-derived human plaque Biobank, contributed to designing and interpretation of the experiments and to editing the manuscript. All authors read and edited the final draft of the manuscript.

**Competing Interest Statement:** AMC is a co-founder and scientific advisor for the autophagy program at Life Biosciences and she consults for Generian Pharmaceuticals and Cognition Therapeutics. JMM is the founder and consults for Instituto Ibions SLP. Dr. Baker was co-author with Dr. Finkel in a review article in 2019. The rest of the authors declare no competing interests in relation with this work.

**Classification:** Biological Sciences > Physiology

**Keywords:** atherosclerotic plaques; lipid challenge; lysosomes; proteolysis; vascular disease

**This PDF file includes:**

Main Text  
Figures 1 to 7  
SI including Figures S1-S8 and Tables S1-6

## Abstract

Chaperone-mediated autophagy (CMA) contributes to regulation of energy homeostasis by timely degradation of enzymes involved in glucose and lipid metabolism. Here, we report reduced CMA activity in vascular smooth muscle cells and macrophages in murine and human arteries in response to atherosclerotic challenges. We show that *in vivo* genetic blockage of CMA worsens atherosclerotic pathology through both systemic and cell-autonomous changes in vascular smooth muscle cells and macrophages, the two main cell types involved in atherogenesis. CMA deficiency promotes dedifferentiation of vascular smooth muscle cells and a pro-inflammatory state in macrophages. Conversely, a genetic mouse model with upregulated CMA shows lower vulnerability to the pro-atherosclerotic challenge. We propose that CMA could be an attractive therapeutic target against cardiovascular diseases.

## Significance Statement

Cardiovascular diseases remain the leading cause of death worldwide, and atherosclerosis the most common source of clinical events. Metabolic changes with aging associate with a concurrent increased risk of both type 2 diabetes and cardiovascular disease, with the former further raising the risk of the latter. The activity of a selective type of autophagy, chaperone-mediated autophagy (CMA), decreases with age or upon dietary excesses. Here we study whether reduced CMA activity increases risk of atherosclerosis in mouse models. We have identified that CMA is upregulated early in response to pro-atherogenic challenges and demonstrate that reduced systemic CMA aggravates the vascular pathology in these conditions. We also provide proof-of-concept support that CMA upregulation is an effective intervention to reduce atherosclerosis severity and progression.

## Main Text

### Introduction

Cardiovascular disease (CVD) is the leading underlying cause of death worldwide accounting for more than 31.5% of total deaths (1). The main risk factors for the development of atherosclerosis - the most common cause of CV clinical events - such as obesity, hypertension, diabetes and aging are rising in epidemic proportions due to changes in lifestyle and the growing elderly population (2). In atherosclerosis, hypercholesterolemia leads to vascular endothelial dysfunction and extravasation of atherogenic lipoproteins, resulting in increased adhesion and extravasation of monocytes from the circulation to the intima (3, 4). Once there, monocytes engulf modified low-density lipoproteins (LDL), differentiate into macrophages and foam cells and proliferate forming a neointima with a lipid-laden macrophage core (5). High cytokine secretion and production of nitric oxide (NO) and reactive oxygen species (ROS) at the lipid-, necrotic-, and macrophage-rich regions creates a pro-inflammatory and oxidative environment that drives dedifferentiation of vascular smooth muscle cells (VSMC) from a contractile to an activated secretory and migratory phenotype (1, 6-8). Activated VSMC migrate from the media into the intima, further increasing inflammation, oxidative stress and collagen and elastin deposition at the fibrous cap (9). The pro-inflammatory, oxidative and hypoxic environment in the plaque exacerbates cellular toxicity and cell death and promotes vascular calcification and matrix degradation (10, 11), which together make the plaque prone to rupture and often result in the subsequent clinical event (12).

Autophagy mediates the degradation of cellular components in lysosomes, thus assuring intracellular quality control and cellular energetics through recycling of essential catabolites (13). Macroautophagy, the most extensively studied type of autophagy, has proven important in endothelial cells (14), VSMC (15) and macrophages (16) for maintenance of the vasculature homeostasis and in the response to lipid challenges and protection against



atherosclerosis (17). In contrast, the role of other autophagy types in vascular cells is less known. Chaperone-mediated autophagy (CMA) is a selective type of autophagy for proteins bearing a pentapeptide motif (KFERQ-like motif) (18, 19). The heat shock cognate protein (HSC70) recognizes this motif and delivers substrate proteins to lysosome-associated membrane protein type 2A (LAMP-2A), that serves as receptor and translocation complex upon multimerization (20, 21). Substrate proteins reach the lysosomal lumen through this complex assisted by the lysosomal-resident HSC70 (22-24). Besides removal of oxidized and damaged proteins by CMA, selective and timely degradation of fully functional proteins by this type of autophagy terminates their function. This regulated remodeling of the proteome by CMA is behind its participation in the regulation of multiple intracellular processes, such as glucose and lipid metabolism, cell cycle, transcriptional programs or T-cell activation, among others (25-27). In fact, *in vivo* blockage of CMA in liver results in exacerbated glycolysis and lipogenesis (25) and blocks lipolysis (26). Although basal levels of CMA are detectable in most mammalian cells, CMA is upregulated in response to proteotoxicity (28), lipotoxicity (29), oxidative stress (30) and hypoxia (31), all conditions that contribute to the etiology of atherosclerosis (9). Reduced CMA activity - due to lower stability and altered LAMP-2A lysosomal dynamics - has been described upon sustained dietary lipid challenges (high fat or cholesterol diets), diabetes and in aging, all major risk factors for CVD (29, 32-34).

The protective role of CMA against mechanisms related to the etiology of CVD motivated us to investigate the possible contribution of CMA failure to the development of atherosclerosis (35). Here, we show that blockage of CMA in mice increases their vulnerability to pro-atherosclerotic challenges, through both systemic and cell-autonomous changes in VSMC and macrophages, the two main cell types involved in atherogenesis. Loss of CMA in VSMC promotes their dedifferentiation and higher susceptibility to lipid challenges, while defective CMA in macrophages leads to a more pro-inflammatory phenotype. We propose that CMA is a defense mechanism activated in the vasculature in response to pro-atherosclerotic challenges and that reduced CMA activity leaves the vasculature vulnerable to these challenges. Using mice with genetically enhanced CMA, we demonstrate that, when exposed to pro-atherosclerotic challenges, they display reduced disease severity and slower progression. Our findings support that CMA could be a therapeutic target for atherosclerosis.

## Results

### **CMA blockage exacerbates atherosclerosis in a murine experimental model**

We used the recently developed transgenic mouse model expressing a fluorescence reporter for CMA (KFERQ-PS-Dendra2 mice) that allows measuring CMA activity *in vivo* (36) to determine the status of CMA in the vasculature and its possible changes during atherosclerotic plaque development. When KFERQ-PS-Dendra CMA substrate is delivered to lysosomes, CMA activity is detected as fluorescent puncta against the diffuse fluorescent cytosolic pattern (36). Using aortas from healthy mice and two-photon microscopy in fixed tissue or intravital two-photon microscopy, we found fluorescent puncta in cells in the media (VSMC) and to less extent in the intima (endothelial cells) (**Figure 1A,B** and **S1A**). Injection of fluorescent dextran that highlights the lysosomal compartment upon internalization from the bloodstream by endocytosis demonstrated colocalization with the Dendra signal in a fraction of lysosomes, in support of active CMA in the vasculature under basal conditions (**Figure 1C**). When we promoted atherosclerosis development in KFERQ-PS-Dendra2 mice through hypercholesterolemia (using injection of adeno-associated virus 8-mediated overexpression of proprotein convertase subtilisin/kexin type 9 (AAV8-PCSK9) and a high cholesterol-containing diet (Western type diet, WD) for 12 weeks), aortas from these mice revealed a marked reduction in the number of fluorescent puncta that was almost absent in the plaque (**Fig. 1D,E** and **S1B** that shows maximal projections throughout the plaque area, with collagen highlighted in red). Co-staining of these atherosclerotic aortas with the VSMC marker  $\alpha$ -smooth muscle actin ( $\alpha$ -sma) and the macrophage marker cluster of differentiation 68 (CD68), revealed almost no CMA activity in either cell type (**Figure S1C**). Immunohistochemistry of the plaque demonstrated that levels of LAMP-2A, the limiting component for CMA, can be detected both in VSMC and macrophages by 6 weeks of plaque formation, but LAMP-2A levels significantly decreased in more advanced stages (12 weeks) of murine atherosclerotic disease in both VSMC and macrophages, in agreement with the observed reduction in CMA activity (**Figures 1F** and **S1D**).

To determine if the initial upregulation of LAMP-2A in response to the dietary challenge was protective and whether reduced CMA contributes to disease progression, we used a mouse model with systemic blockage of CMA (constitutive knock-out for LAMP-2A, L2AKO (37)) (**Figure S1E**). At 3 months of age, L2AKO mice on chow diet display slightly lower body weight and circulating total cholesterol levels than wild-type (WT) littermates (**Figure S1F,G**). When L2AKO mice were fed WD for 12 weeks, we observed a marked increase in total circulating cholesterol and triglyceride (TG) levels (**Figure 1G,H**), mainly in the very-low-density lipoprotein (VLDL) and LDL fractions (**Figure 1I,J**). Atherosclerotic plaques in the aortic root of L2AKO mice were larger than in WT mice (approx. 39%) (**Figure 1K,L**), with a noticeable trend toward bigger necrotic cores, lower cellularity and significantly more advanced plaques (**Figures 1M,N** and **S1H**). Plaques in the CMA-incompetent mice also had more collagen content, thicker fibrous cap, yet higher abundance of calcifications (**Figures 1O-R** and **S1I**). In addition, the relative contents of both  $\alpha$ -SMA for contractile VSMC and CD68+ for macrophages in the plaque were significantly lower in L2AKO mice (**Figure 1S,T**).

Overall, reduced CMA activity associates with many aspects of more severe atherosclerotic pathology supporting an anti-atherosclerotic protective function for CMA.

### **Metabolic dysfunction in CMA-deficient mice**

To determine the basis for the protective effect of CMA against atherosclerosis, and because of the previously described regulation of hepatic glucose and lipid metabolism by CMA (25), we evaluated metabolic parameters shown to be major risks factors for CVD. We found that L2AKO mice gained 50% more body weight than the WT group during the 12 weeks of WD (**Figure 2A**), mostly due to a higher fat mass content (**Figure 2B** and **S2A**). Indirect calorimetry revealed that the increased adiposity of L2AKO mice did not originate from higher food consumption (**Figure 2C** and **S2B,C**), but it could be explained by reduced energy expenditure (**Figure 2D** and **S2D,E**) and less physical activity (**Figure 2E**). The decrease in respiratory exchange ratio (RER) -

indicative of lipid use as energy - observed in WT mice on WD was significantly more pronounced in L2AKO mice (**Figure S2F**), suggesting impaired carbohydrate utilization in these mice. Indeed, L2AKO mice showed marked hyperinsulinemia (**Figure 2F**) and increased insulin resistance (**Figure 2G,H**), typical risk factors for CVD (38). Circulating levels of the pro-thrombotic and pro-fibrotic cytokine plasminogen activator inhibitor type 1 (PAI-1) were also significantly higher in L2AKO mice (**Figure 2I**). These findings support that loss of CMA accentuates the systemic derangements in metabolism and coagulation imposed by the WD, thus rendering organisms more prone to atherosclerosis.

### **CMA blockage promotes VSMC dedifferentiation**

Whereas circulating cholesterol levels in WT mice show the previously described correlation with different plaque properties, such correlations are lost in L2AKO mice (**Figure 2J-M**). This suggests that factors other than systemic metabolic changes also contribute to the higher vulnerability of L2AKO mice to atherosclerosis. This motivated us to investigate whether local changes of CMA in the vasculature could contribute to disease progression.

We first examined CMA in primary cultured VSMC exposed to a physiological lipid challenge (LDL loading) and found a dose-dependent upregulation of CMA followed by a gradual decrease once toxic concentrations of LDL are reached (**Figure 3A and S3A**). Exposure of L2AKO VSMC (**Figure S3B**) to fluorescent LDL (diLDL) resulted in higher intracellular lipid accumulation (**Figure 3B**) and reduced cellular viability as LDL concentrations increased (**Figure 3C**). This higher susceptibility to lipotoxicity can be primarily attributed to the loss of CMA, since other types of autophagy (i.e., macroautophagy shown in **Figure S3C-F**) were fully functional in these cells.

Comparative analysis of the transcriptional profile of WT and L2AKO VSMC revealed marked differences under basal conditions and an inadequate transcriptional response after exposure to LDL in L2AKO cells (**Figure 3D and S4A-C**). Under basal conditions L2AKO VSMC exhibited loss of ACTA2, an activated-macrophage like gene profile and acquisition of recently identified markers of modified, dedifferentiated VSMC (8) (**Figure 3D and S4D**). These findings are in line with loss of ACTA2<sup>+</sup> contractile SMCs in the plaques *in vivo* (**Figure 1S**). Gene set enrichment analysis (with STRING database) further showed upregulation of nodes related to cell migration, proliferation, differentiation and response to lipids (**Figure S4E**).

Loading with LDL induced changes in genes related to lipid metabolism in both genotypes (**Figure S4F**), but we identified quantitative differences in this response. Thus, using Ingenuity Pathway Analysis (IPA), we found that L2AKO cells have a defective response to the lipid challenge with reduced upregulation of genes involved in the cholesterol pathway and display cholesterol as one of the top molecules upregulated in these cells (**Figure S4G**). The immune component of the response of VSMC to lipids is also different in L2AKO cells. While WT cells orchestrate a well-characterized inflammatory response, the immune response of L2AKO cells is mainly composed of genes related to leucocyte activation and cell migration (**Figure S4F**). Differential gene expression analysis and gene set enrichment upon lipid loading also identified gene nodes unique for L2AKO cells related with cell death and cellular response to stress, including the response to DNA damage (**Figure 3E**), which we experimentally confirmed to be significantly increased in these cells (**Figure 3F,G**). These findings support that failure to activate CMA in VSMC makes them unable to adapt to the environmental lipid challenge, as previously described also in CMA-deficient hepatocytes (25).

Analysis of upstream regulators of the group of genes differentially expressed in L2AKO VSMC revealed as the top change a significant ( $p < 3.13 \times 10^{-46}$ ) downregulation of the tumor protein 53 (p53) signaling pathway (**Figure 3E**). Immunoblot against different components of the p53 signaling pathways confirmed markedly reduced levels of p53 protein and of the cyclin-dependent kinase inhibitor 1A (p21) in L2AKO VSMC, whereas cyclin-dependent kinase inhibitor 1B (p27) content was higher in these cells compared with WT (**Figure 3H**). In light of the well-characterized role of p53 as anti-apoptotic molecule in response to lipid challenges, the identified defect in p53

signaling in L2AKO VSMC provides an explanation for their higher death count (**Figure 3C**), increased DNA damage (**Figure 3F,G**) and higher proliferation rates (**Figure 3I**) upon LDL loading. Furthermore, relevant to this study is the fact that p53 has previously been shown to protect against VSMC dedifferentiation (39), a transcriptional pattern already noticeable in L2AKO VSMC under basal conditions (**Figure 3D**).

We also detected that L2AKO VSMC show constitutively higher intracellular content of the pro-inflammatory and damage-danger-associated molecule pattern (DAMP) chaperone high mobility group box protein-1 (HMGB1) (**Figure S4H**), known to complex with p53 (40, 41) and to stimulate PAI-1 (42). Even more striking was the augmented release of HMGB1 into the extracellular media in the form of large molecular weight complexes (**Figure 3J**). This continuous release of HMGB1 from L2AKO VSMC in the arterial wall may be one of the major drivers of the local inflammation and calcium deposition observed in the aortas of L2AKO mice (**Figure 1R** and **Figure S1I**) and may also contribute to perpetuate dedifferentiation of CMA-defective VSMC. Also, as part of the possible impact of L2AKO VSMC in arterial wall, and in agreement with our *in vivo* observations (**Figure 1O,P**), we found a marked increase in most of collagen genes previously associated with plaque fibrosis (**Figure 3K**), which further supports VSMC transition into a synthetic phenotype.

Our findings in L2AKO VSMC confirm that fully functional CMA is required in their defense against lipotoxicity and to maintain the identity of VSMC by preventing their dedifferentiation into secretory-migratory cells.

#### **Pro-inflammatory phenotype of CMA-defective macrophages**

The presence of macrophages in the plaque and their associated inflammatory phenotype influence plaque fate. Therefore, we next set to investigate the consequences of CMA blockage in macrophage function using *in vitro* protocols for polarization of bone marrow-derived macrophages (BMDM) to mimic the plaque pro-inflammatory phenotype of these cells (IFN $\gamma$ +LPS). We found that CMA-defective BMDM, when stimulated with IFN $\gamma$ +LPS, show a stronger pro-inflammatory profile (higher inducible nitric oxide synthase, iNOS, and cytochrome c oxidase 2 (COX2) levels (**Figure 4A-C** and **S5A,B**) suggesting that CMA may modulate pro-inflammatory polarization of macrophages. Interestingly, although the changes in COX2 levels were in large part due to its transcriptional upregulation, in the case of iNOS the increase was only at the level of protein, in support of changes in protein degradation contributing to the observed elevated cellular iNOS levels (**Figure 4A-C**). We did not observe differences in macroautophagic activity between WT and L2AKO BMDM (**Figure S5C**), in support of the observed phenotype being primarily a consequence of loss of CMA.

We aimed to identify the subset of the proteome that, by not undergoing degradation through CMA, could be behind this exacerbated inflammatory phenotype seen in the L2AKO BMDM. Thus, we isolated the pool of lysosomes usually active for CMA, those that contain high levels of luminal HSC70, from WT and L2AKO BMDM, untreated (CTRL) or stimulated with IFN $\gamma$ +LPS. In half of the cultures, we inhibited lysosomal proteolysis to discriminate proteins undergoing degradation inside lysosomes from lysosomal resident proteins (**Figure 4D** and **S5D**) and subjected the samples to comparative quantitative proteomics (25). About 45% of the proteins were constitutive lysosomal components, not degraded in lysosomes in resting or stimulated BMDM (**Figure 4E**). CMA substrates are defined as those proteins undergoing degradation in lysosomes in a LAMP-2A-dependent manner (**Figure 4D** and **S5E,F**). Stimulation with IFN $\gamma$ +LPS resulted in an increase of lysosomal protein degradation, mostly of CMA substrates (46% increase in CMA substrates vs. only 15% increase in non-CMA lysosomal substrates; **Figure 4F**). In addition, the repertoire of CMA substrates degraded by untreated and stimulated BMDM was largely different, with only 7% coinciding proteins (**Figure 4G**). Data mining using STRING and IPA identified that the top cellular pathways associated with unstimulated macrophages were related with regulation of immune response, cell adhesion molecules and leucocyte activation, besides the expected upregulation of the pro-inflammatory LPS signaling pathway (**Figures 4H** and **S5G**). The

IFN $\gamma$ +LPS treatment induced CMA degradation of nitric oxide synthase along with five other stimulators of NO synthesis (**Figure 4I**), which can explain the higher levels of iNOS in CMA-incompetent macrophages upon stimulation (**Figure 4A,B**). CMA substrates in this condition also included proteins involved in immune response, neutrophil degradation and transendothelial migration (including cell adhesion, cellular localization and interaction with the vascular wall) (**Figures 4J** and **S5H**). The *in vivo* data confirmed these findings since we found that L2AKO mice showed marked monocytosis, mainly derived from a higher number of proinflammatory monocytes (**Figure 4K,L**), and elevated number of T-cells, especially CD4<sup>+</sup> T-cells (**Figure 4M,N** and full blood leucocyte pattern in the same mice shown in **Table S1**).

Overall, our findings support that CMA contributes to the remodeling of the proteome induced by macrophage stimulation, and that defective CMA in these cells promotes a more pro-inflammatory phenotype.

### **Human carotid CMA response to pro-atherosclerotic conditions**

Our *in vitro* and *in vivo* findings support that CMA upregulation may be part of the vascular response to pro-atherosclerotic challenges. To test whether that was also the case in human atherosclerosis we have used four different human datasets (clinical characteristics for the different human cohorts in this section are described in SI and **Tables S2, S3**). We first confirmed the presence of the CMA receptor in plaque VSMC and macrophages using co-staining for LAMP-2A and  $\alpha$ SMA/CD68 (**Figure 5A,B**; details in SI (study 1)). Analysis of levels of LAMP-2A in human autopsy-derived atherosclerotic plaques from asymptomatic patients at different plaque stages revealed that LAMP-2A levels at the plaque increase gradually with disease progression (graded as plaques with moderate intimal thickening (IT), pathological intimal thickening (PIT), thick fibrous cap atheroma (TkFCA) and plaques with intraplaque hemorrhage (IPH)) (**Figure 5C,D**). Similarly, LAMP-2A mRNA levels in carotid plaques, surgically retrieved from symptomatic patients (from (43), details in SI (study 2)) directly correlated with the size of the plaque but not the necrotic core (**Figure 5E,F**). To determine the cell type mainly contributing to the elevated levels of LAMP-2A in the plaque, we analyzed the correlation between LAMP-2A mRNA levels and different cell types and found a direct correlation between LAMP-2A and CD68, a marker of macrophages and foam cells, in human atherosclerotic plaques (**Figure 5G,H**). We interpreted these changes in LAMP-2A levels as an attempt of the plaque cells, mostly macrophages, to upregulate this autophagic pathway in response to the pro-atherosclerotic changes prior to clinical events, as we observed in the experimental mouse model (**Figure 1D**). In fact, holistic analysis of the CMA transcriptional network using single cell RNA seq (scRNAseq) from human coronary atherosclerotic plaques (from (8), details in SI (study 3)) confirmed macrophages as the cells with the highest expression of CMA effectors (LAMP-2A and HSC70) when compared to endothelial and smooth muscle cells from the same plaques (**Figures 5I** and **S6A,B**).

To evaluate possible changes of CMA after the clinical event, we performed immunoblot for LAMP2 in carotid segments retrieved from surgery in patients who suffered one event at baseline or an additional clinical vascular event at follow-up (details in SI (study 4) and **Tables S2, S3**). This revealed a significant decrease in LAMP2 levels in carotid segments from all patients who develop a second event (**Figure 5J**). This decrease in LAMP2, seems to be driven mostly by the female patients in this group, that were the ones displaying the most pronounced changes in overall LAMP2 content (**Figures 5K** and **S6C,D**). Changes cannot be attributed to differences in patient's ages that were  $66.1 \pm 3.4$  and  $70.4 \pm 3.8$  for first and second event, respectively in female patients and  $65.6 \pm 1.3$  and  $74.3 \pm 1.2$  for the same groups in male patients. Indeed, sex-stratified logistic regression confirmed a significant association of LAMP2A with an additional clinical event, and with time to event in women (n=22), independent of age, BMI or hypertension, but not in men (n=37, **Table S4, S5**). Although this study is not sufficiently powered to discard other confounding effects, we did not find direct correlations of LAMP2 levels and any of the available clinical parameters (**Figure S6F-J**). The observed changes, seem selective for LAMP2, rather than an overall reduction in the lysosomal content, since levels of

cathepsin D, another lysosomal marker, remained unchanged (**Figure 5J,K** and **S6C,E**). We have recently developed and validated an algorithm that allows inferring CMA activity based on the weighted averaged expression of the genes known to contribute as effectors or regulators to CMA (**Figure S6A**). Analysis of the CMA score using transcriptomics from patient plaques predicted reduction of CMA activity in unstable atherosclerotic plaques when compared with stable ones (study 2, **Figure 5L**). Deconvolution analysis highlighted an overall lower expression of most network elements, especially of positive lysosomal modulators, despite an increase of effectors (LAMP-2A and HSC70) (**Figure 5M**). This increase in LAMP-2A mRNA can be interpreted as an attempt to compensate for the pronounced decrease in LAMP2A protein levels in these patients, likely due to reduced stability of this protein as previously observed upon persistent lipid challenges (29).

These findings support that atherosclerotic disease also associates with dysfunctional CMA in the vasculature in humans.

### **CMA upregulation protects against atherosclerosis in mice**

To experimentally test the proposed protective effect of CMA activation - observed early in the disease in mice and in human plaques - and to evaluate the possible therapeutic value of CMA modulation in atherosclerosis, we directly upregulated CMA activity in mice exposed to a pro-atherosclerotic challenge. To that end, we used an inducible transgenic mouse model (hL2AOE), expressing the human form of LAMP-2A (44) (**Figure S1E**), which we induced after the observed drop in LAMP-2A levels in early plaques (**Figures 1E** and **S7A**). We confirmed that weight and circulating cholesterol were indistinguishable between WT and hL2AOE mice before the treatment (**Figure S1F,G**). After the pro-atherosclerotic challenge, although circulating cholesterol and triglyceride levels were only discretely reduced, increasing CMA activity markedly decreased the fraction of both lipids in the VLDL and LDL fractions (**Figure 6A-D**). As anticipated, the improved lipid profile of the hL2AOE group associated with an increase in insulin sensitivity (**Figure 6E**). The hL2AOE mice also showed a trend towards ameliorated profile of multiple pro-inflammatory cytokines (i.e., PAI1, CCL3, 4 and G-CSF shown in **Figure S7B,D,F**) that we found modified in the opposite direction in CMA-defective mice upon the same challenge (**Figures 2I** and **S7C,E**). Analysis of the atherosclerotic plaque revealed that hL2AOE mice exhibited smaller lesions with reduced necrotic cores and less calcification (**Figure 6F-J**) although collagen content, plaque stage and number of VSMC and macrophages were comparable in both groups of mice (**Figure 6K,L** and **S7G-J**). Principal component analysis with 12 variable data shows that Ctrl and hL2AOE mice groups are distributed in different regions in support of these groups evolving differently upon the lipid challenge (**Figures 6M,N** and **S7K**).

Overall, these findings support both systemic and vascular beneficial effects of CMA upregulation and highlight the therapeutic potential of activating CMA to prevent atherosclerotic disease progression.

## Discussion

In this work, we have identified a protective role for CMA against atherosclerotic disease through a combination of systemic and local effects. Fully functional CMA protects against systemic changes that promote disease progression, such as levels of circulating lipids, glucose metabolism and immune-inflammatory response. In addition, CMA in cells in the vasculature and the plaque reduces lesion severity by preserving VSMC identity and modulating the macrophage pro-inflammatory phenotype. The aggravated atherosclerotic pathology observed upon CMA blockage *in vivo* underscores the contribution to disease progression. We propose that upregulation of CMA is part of the organism's response to pro-atherogenic challenges, but that factors such as aging or sustained dietary pressure, known to inhibit CMA, reduce the efficacy of this protective mechanism. We show that genetic activation of CMA slows down disease progression in mice supporting a potential therapeutic value of CMA upregulation in atherosclerosis.

We favored for our study systemic disruption of CMA to better recapitulate the overall reduced CMA activity observed in aging (32) or upon dietary lipid challenges (29). In fact, although functional CMA studies in humans are still not feasible, analysis of the expression of the CMA network genes in aortas from healthy individuals of different ages (from the GTEx aging database), predicted a gradual decrease with age in their overall CMA score (**Figure S8A**). This decrease does not seem to be related to decreased lysosomal biogenesis because while LAMP2A expression was reduced in the older groups, expression of other lysosomal proteins such as LAMP1 increased with age (**Figure S8B**). Single cell RNAseq of human aortas from the Tabula Sapiens cell atlas (45), supported a similar trend of CMA decrease with age, albeit at different rates, preferentially in macrophages and VSMC (**Figure S8C-F**).

As expected of a protein degradation pathway with the potential to degrade more than 45% of cytosolic proteins (those with KFERQ-like motifs (19)), the mechanisms behind protective effect of CMA against atherosclerosis are multiple. Our findings support a systemic role for CMA in regulation of organismal metabolism. Blockage of CMA in liver leads to profound metabolic derangements due to failure to timely degrade proteins involved in glucose and lipid metabolism (26). Defective liver metabolism in the mice with systemic CMA blockage used in this study may be responsible for the abnormal cholesterol and lipoproteins profiles observed in these mice upon lipid challenge (46). Furthermore, these mice phenocopy part of the aging metabolic phenotype characterized by diminished aerobic capacity (47) and insulin resistance due to abdominal adiposity (38). Several systemic changes observed in the L2AKO mice (hypercholesterolemia, hypertriglyceridemia, insulin resistance and elevated acute phase proteins such as PAI-1 (48)) are major risk factors for atherosclerosis in humans and may contribute to the aggravating effect of CMA failure on the disease. However, our studies with isolated primary cells, also highlight that part of the protective effect of CMA occurs directly at the vascular wall.

Previous studies support a relationship between autophagy, mainly macroautophagy, and atherogenesis, that resembles in many aspects the one described here for CMA. Preclinical studies have shown that VSMC upregulate macroautophagy in response to several pro-atherogenic stimuli, such as lipids, proinflammatory cytokines, growth factors and/or oxidative stress (49), whereas autophagic malfunction leads to VSMC phenotype switch and foam cell formation (15, 50, 51). In fact, mice knock out for the essential autophagy gene ATG7 in VSMC show impaired mitophagy, increased oxidative stress and apoptosis, all hallmarks of advanced vulnerable atherosclerotic plaques (52). A similar protective effect of macroautophagy against lipid challenges has also been described in the endothelial cells (14) and macrophages (16) whereas specific blockade of macroautophagy in macrophages *in vivo* leads to atherosclerosis progression (53, 54). We identified similar functions for CMA in VSMC and macrophages in the context of pro-atherosclerotic stimuli to the ones described for macroautophagy. Nevertheless, these pathways are non-redundant, since blockage of only one of them is sufficient to aggravate disease progression. These findings highlight rather the complementarity between these autophagic pathways, which likely originates from their different mechanisms of action. For example, while the protective effect of macroautophagy against lipotoxicity is attained in large

part through active degradation of lipid stores through lipophagy (16), we show in this work that CMA protects against lipotoxicity through regulation of the cholesterol biosynthetic pathway, by combined selective degradation of cholesterol biogenic enzymes and of transcription factors that mediate activation of these pathways.

We also found that failure to activate CMA in response to lipid challenges is sufficient to promote a dedifferentiated-activated like phenotype in VSMC, an essential step in atherosclerosis etiology and development (7). In fact, the large, fibrous and calcified plaques with extensive necrosis observed in L2AKO mice are representative of a mature stage of atherosclerosis progression that develops with aging (55) (AHA classification types Vc and Vb, or fibrocalcific plaque according to Virmani's (12)). We propose that impaired timely degradation by CMA of the identified intracellular signaling proteins is behind the reduced viability and failure to preserve cellular identity in CMA-defective VSMC. For example, reduced p53 signaling can explain the higher cellular proliferation, DNA damage and HMGB1 release and higher cell death rates observed in CMA-deficient VSMC upon LDL loading.

The other cellular component of the atherosclerotic plaque directly affected by changes in CMA activity are macrophages. We found quantitative and qualitative changes in the subproteome degraded by CMA during the macrophage phenotypic switch and that defective CMA under these conditions leads to an aberrant pro-inflammatory phenotype in these cells. Among the novel CMA substrates in stimulated macrophages identified in this work, proteins involved in NO synthesis, leucocyte activation and migration, cell adhesion, neutrophil degranulation and LPS signaling have all been tightly connected with development of atherosclerosis (56, 57).

CMA is activated in response to lipotoxic stimuli, oxidative stress and hypoxia (29-31), all co-existing conditions at the atherosclerotic plaque (4, 58, 59). We propose that the high levels of LAMP-2A identified with human plaque progression in asymptomatic subjects may be indicative of reactive CMA upregulation, as the one observed in mice in the early stages of the pro-atherosclerotic challenge, to protect against later events in the human disease. In fact, a similar compensatory upregulation, as an attempt to overcome the pathology, has also been proposed for macroautophagy in atherosclerotic patients. Ultrastructural studies in human aorta demonstrated autophagosome-like structures in atherosclerotic lesions (60) and expression of autophagy markers, such as the autophagy initiator ATG16L1, have been found increased in atherosclerotic plaques and correlate with plaque vulnerability (61). It is likely that these compensatory mechanisms, when sustained for a long period of time, may be insufficient or even no longer triggered. The reduced overall CMA score that we predicted from the transcriptional profile of advanced plaques in human aorta when compared to early plaques supports this possibility. To date, the only genetic link between CMA and cardiovascular conditions in humans is with the vacuolar cardiomyopathy Danon's Disease, where patients harbor mutations in the *lamp2* gene (62). Genome-wide association studies have reported SNPs for several components of the CMA network with cardiovascular and metabolic conditions (63, 64), but since those genes also participate in other cellular processes, future experimental testing will be required to explore their direct impact on CMA.

Although future studies on the status of CMA at the different disease stages in patients are needed to determine the possible timeframe of the efficacy of this intervention in humans, our work provides proof of concept for the therapeutic value of CMA upregulation in atherosclerosis. Malfunctioning of both macroautophagy (54, 65, 66) and CMA (this work) have been reported in atherosclerosis disease. Interestingly, genetic upregulation *in vivo* of either of them, by overexpressing the positive regulator of macroautophagy TFEB (66) or the limiting CMA component LAMP2A (this work), successfully slow down atherosclerotic disease progression in mice. These findings and the mechanistic complementarity between both pathways provide rationale for a possible beneficial additive effect of combinatorial therapeutics targeting both pathways.



## Materials and Methods

### Animal models and primary cultures

All mouse models used in this work and the procedures to generate primary cultures of VSMC and BMDM from those models are described in detail in *SI Appendix, SI Material and Methods*.

### Metabolic analysis

Plasma total cholesterol (TC) (Cholesterol E, 999-02601, Wako) and triglycerides (TG) (L-Type Triglyceride M, 992-02892 and 998-02992, Wako) were assessed using standard enzymatic assays automated on the Infinite 200-Pro (Tecan). Body weight, body composition and calorimetric data were acquired open-circuit indirect calorimetry system and are further described in *SI Appendix, SI Material and Methods*

### Image analysis

For immunohistochemistry, aortic roots were serially sectioned and stained with colorimetric stains or with primary antibodies and their corresponding fluorescence-conjugated secondary antibodies to visualize specific proteins. Direct Dendra fluorescence in KFERQ-Dendra2 mice was visualized using two photon and intravital microscopy as described in detail in *SI Appendix, SI Material and Methods*.

### CMA activity

CMA activity was analyzed with fluorescence reporters as described before (67) (36) or by analysis of the transcriptional changes in the genes of CMA effectors and regulators (CMA network) using the CMA score algorithm previously described and validated in ref. (68)

## Acknowledgments

We thank Trea Streefland (LUMC) for her assistance with generating the lipid profiles and Jacques Debets and Clairij Dinjens (MUMC) for assistance with sectioning and immunohistochemistry. The Genotype-Tissue Expression (GTEx) Project used for the calculations of CMA scores was supported by the Common Fund of the Office of the Director of the NIH and the Tabula Sapiens project, used for the same purpose, was supported by the grant 2019-203354 from the Chan Zuckerberg Initiative DAF. This work was supported by National Institutes of Health grants AG021904 and DK098408 (to AMC), AG031782 (to AMC, RS, JBC and FM), the A15CVD04 Leducq Foundation Network (to AMC and JCS), and a Dr. Dekker senior postdoc fellowship from the Dutch Heart Foundation (2016T060 to JCS). JMM was supported by a postdoctoral fellowship from the American Heart Association 17POST33650088, AM-S by a Ramon Areces Postdoctoral Fellowship and GJK by TGT32GM007288 and T32GM007491.

## References

1. S. S. Virani *et al.*, Heart Disease and Stroke Statistics-2021 Update: A Report From the American Heart Association. *Circulation* **143**, e254-e743 (2021).
2. E. J. Benjamin *et al.*, Heart Disease and Stroke Statistics-2017 Update: A Report From the American Heart Association. *Circulation* **135**, e146-e603 (2017).
3. P. Libby, The changing landscape of atherosclerosis. *Nature* **592**, 524-533 (2021).
4. I. Tabas, K. J. Williams, J. Boren, Subendothelial lipoprotein retention as the initiating process in atherosclerosis: update and therapeutic implications. *Circulation* **116**, 1832-1844 (2007).

5. K. J. Moore, I. Tabas, Macrophages in the pathogenesis of atherosclerosis. *Cell* **145**, 341-355 (2011).
6. Y. Vengrenyuk *et al.*, Cholesterol loading reprograms the microRNA-143/145-myocardin axis to convert aortic smooth muscle cells to a dysfunctional macrophage-like phenotype. *Arterioscler Thromb Vasc Biol* **35**, 535-546 (2015).
7. M. R. Bennett, S. Sinha, G. K. Owens, Vascular Smooth Muscle Cells in Atherosclerosis. *Circ Res* **118**, 692-702 (2016).
8. R. C. Wirka *et al.*, Atheroprotective roles of smooth muscle cell phenotypic modulation and the TCF21 disease gene as revealed by single-cell analysis. *Nat Med* **25**, 1280+ (2019).
9. P. Libby, Vascular biology of atherosclerosis: overview and state of the art. *Am J Cardiol* **91**, 3A-6A (2003).
10. M. J. Mitchinson, S. J. Hardwick, M. R. Bennett, Cell death in atherosclerotic plaques. *Curr Opin Lipidol* **7**, 324-329 (1996).
11. D. Proudfoot *et al.*, Apoptosis regulates human vascular calcification in vitro: evidence for initiation of vascular calcification by apoptotic bodies. *Circ Res* **87**, 1055-1062 (2000).
12. R. Virmani, F. D. Kolodgie, A. P. Burke, A. Farb, S. M. Schwartz, Lessons from sudden coronary death: a comprehensive morphological classification scheme for atherosclerotic lesions. *Arterioscler Thromb Vasc Biol* **20**, 1262-1275 (2000).
13. N. Mizushima, M. Komatsu, Autophagy: renovation of cells and tissues. *Cell* **147**, 728-741 (2011).
14. K. Torisu *et al.*, Intact endothelial autophagy is required to maintain vascular lipid homeostasis. *Aging cell* **15**, 187-191 (2016).
15. M. O. Grootaert *et al.*, Defective autophagy in vascular smooth muscle cells accelerates senescence and promotes neointima formation and atherogenesis. *Autophagy* **11**, 2014-2032 (2015).
16. M. Ouimet *et al.*, Autophagy regulates cholesterol efflux from macrophage foam cells via lysosomal acid lipase. *Cell Metab* **13**, 655-667 (2011).
17. J. M. Henderson, C. Weber, D. Santovito, Beyond Self-Recycling: Cell-Specific Role of Autophagy in Atherosclerosis. *Cells* **10** (2021).
18. J. F. Dice, Peptide sequences that target cytosolic proteins for lysosomal proteolysis. *Trends Biochem Sci* **15**, 305-309 (1990).
19. P. Kirchner *et al.*, Proteome-wide analysis of chaperone-mediated autophagy targeting motifs. *PLoS Biol* **17**, e3000301 (2019).
20. H. Chiang, S. Terlecky, C. Plant, J. F. Dice, A role for a 70-kilodalton heat shock protein in lysosomal degradation of intracellular proteins. *Science* **246**, 382-385 (1989).
21. A. M. Cuervo, J. F. Dice, A receptor for the selective uptake and degradation of proteins by lysosomes. *Science* **273**, 501-503 (1996).
22. U. Bandyopadhyay, S. Kaushik, L. Varticovski, A. M. Cuervo, The chaperone-mediated autophagy receptor organizes in dynamic protein complexes at the lysosomal membrane. *Mol Cell Biol* **28**, 5747-5763 (2008).
23. F. A. Agarraberes, S. R. Terlecky, J. F. Dice, An intralysosomal hsp70 is required for a selective pathway of lysosomal protein degradation. *J Cell Biol* **137**, 825-834 (1997).

24. N. Salvador, C. Aguado, M. Horst, E. Knecht, Import of a cytosolic protein into lysosomes by chaperone-mediated autophagy depends on its folding state. *J Biol Chem* **275**, 27447-27456 (2000).
25. J. L. Schneider, Y. Suh, A. M. Cuervo, Deficient chaperone-mediated autophagy in liver leads to metabolic dysregulation. *Cell Metab* **20**, 417-432 (2014).
26. S. Kaushik, A. M. Cuervo, Degradation of lipid droplet-associated proteins by chaperone-mediated autophagy facilitates lipolysis. *Nature cell biology* **17**, 759-770 (2015).
27. R. Valdor *et al.*, Chaperone-mediated autophagy regulates T cell responses through targeted degradation of negative regulators of T cell activation. *Nature immunology* **15**, 1046-1054 (2014).
28. A. M. Cuervo, H. Hildebrand, E. M. Bomhard, J. F. Dice, Direct lysosomal uptake of alpha 2-microglobulin contributes to chemically induced nephropathy. *Kidney Int* **55**, 529-545 (1999).
29. J. A. Rodriguez-Navarro *et al.*, Inhibitory effect of dietary lipids on chaperone-mediated autophagy. *Proc Natl Acad Sci U S A* **109**, E705-714 (2012).
30. R. Kiffin, C. Christian, E. Knecht, A. M. Cuervo, Activation of chaperone-mediated autophagy during oxidative stress. *Molecular biology of the cell* **15**, 4829-4840 (2004).
31. E. Dohi *et al.*, Hypoxic stress activates chaperone-mediated autophagy and modulates neuronal cell survival. *Neurochem Int* **60**, 431-442 (2012).
32. A. M. Cuervo, J. F. Dice, Age-related decline in chaperone-mediated autophagy. *J Biol Chem* **275**, 31505-31513 (2000).
33. R. Kiffin *et al.*, Altered dynamics of the lysosomal receptor for chaperone-mediated autophagy with age. *J Cell Sci* **120**, 782-791 (2007).
34. S. Sooparb, S. R. Price, J. Shaoguang, H. A. Franch, Suppression of chaperone-mediated autophagy in the renal cortex during acute diabetes mellitus. *Kidney Int* **65**, 2135-2144 (2004).
35. J. Madrigal-Matute, L. Scorrano, J. Sadoshima, Leducq Network: Modulating Autophagy to Treat Cardiovascular Disease. *Circ Res* **123**, 323-325 (2018).
36. S. Dong *et al.*, Monitoring spatio-temporal changes in chaperone-mediated autophagy *in vivo*. *Nat. Comm.* **15**, doi: 10.1186/s13024-13019-10354-13020 (2020).
37. J. L. Schneider *et al.*, Loss of hepatic chaperone-mediated autophagy accelerates proteostasis failure in aging. *Aging Cell* **14**, 249-264 (2015).
38. W. M. Kohrt *et al.*, Insulin resistance in aging is related to abdominal obesity. *Diabetes* **42**, 273-281 (1993).
39. Z. Tan *et al.*, P53 Promotes Retinoid Acid-induced Smooth Muscle Cell Differentiation by Targeting Myocardin. *Stem Cells Dev* **27**, 534-544 (2018).
40. A. R. Davalos *et al.*, p53-dependent release of Alarmin HMGB1 is a central mediator of senescent phenotypes. *J Cell Biol* **201**, 613-629 (2013).
41. M. Stros, E. Muselikova-Polanska, S. Pospisilova, F. Strauss, High-affinity binding of tumor-suppressor protein p53 and HMGB1 to hemicatenated DNA loops. *Biochemistry* **43**, 7215-7225 (2004).
42. M. Parra, M. Jardi, M. Koziczak, Y. Nagamine, P. Munoz-Canoves, p53 Phosphorylation at serine 15 is required for transcriptional induction of the plasminogen activator inhibitor-1 (PAI-1) gene by the alkylating agent N-methyl-N'-nitro-N-nitrosoguanidine. *J Biol Chem* **276**, 36303-36310 (2001).

43. H. Jin *et al.*, Integrative multiomics analysis of human atherosclerosis reveals a serum response factor-driven network associated with intraplaque hemorrhage. *Clin Transl Med* **11**, e458 (2021).
44. I. Tasset *et al.*, Anti-aging effects of systemic restoration of chaperone-mediated autophagy. (*in preparation*).
45. T. T. S. Consortium, S. R. Quake, The Tabula Sapiens: a multiple organ single cell transcriptomic atlas of humans. *bioRxiv* 10.1101/2021.07.19.452956, 2021.2007.2019.452956 (2021).
46. J. L. Goldstein, M. S. Brown, A century of cholesterol and coronaries: from plaques to genes to statins. *Cell* **161**, 161-172 (2015).
47. J. L. Fleg *et al.*, Accelerated longitudinal decline of aerobic capacity in healthy older adults. *Circulation* **112**, 674-682 (2005).
48. A. Festa *et al.*, Relative contribution of insulin and its precursors to fibrinogen and PAI-1 in a large population with different states of glucose tolerance. The Insulin Resistance Atherosclerosis Study (IRAS). *Arterioscler Thromb Vasc Biol* **19**, 562-568 (1999).
49. M. O. J. Grootaert *et al.*, Vascular smooth muscle cell death, autophagy and senescence in atherosclerosis. *Cardiovasc Res* **114**, 622-634 (2018).
50. S. Pi *et al.*, The P2RY12 receptor promotes VSMC-derived foam cell formation by inhibiting autophagy in advanced atherosclerosis. *Autophagy* **17**, 980-1000 (2021).
51. J. K. Salabei *et al.*, PDGF-mediated autophagy regulates vascular smooth muscle cell phenotype and resistance to oxidative stress. *Biochem J* **451**, 375-388 (2013).
52. H. Nahapetyan *et al.*, Altered mitochondrial quality control in Atg7-deficient VSMCs promotes enhanced apoptosis and is linked to unstable atherosclerotic plaque phenotype. *Cell Death Dis* **10**, 119 (2019).
53. X. Liao *et al.*, Macrophage autophagy plays a protective role in advanced atherosclerosis. *Cell Metab* **15**, 545-553 (2012).
54. B. Razani *et al.*, Autophagy links inflammasomes to atherosclerotic progression. *Cell Metab* **15**, 534-544 (2012).
55. G. W. van Lammeren *et al.*, Atherosclerotic plaque vulnerability as an explanation for the increased risk of stroke in elderly undergoing carotid artery stenting. *Stroke* **42**, 2550-2555 (2011).
56. M. E. Burleigh *et al.*, Cyclooxygenase-2 promotes early atherosclerotic lesion formation in LDL receptor-deficient mice. *Circulation* **105**, 1816-1823 (2002).
57. P. A. Detmers *et al.*, Deficiency in inducible nitric oxide synthase results in reduced atherosclerosis in apolipoprotein E-deficient mice. *J Immunol* **165**, 3430-3435 (2000).
58. J. L. Martin-Ventura *et al.*, Erythrocytes, leukocytes and platelets as a source of oxidative stress in chronic vascular diseases: detoxifying mechanisms and potential therapeutic options. *Thromb Haemost* **108**, 435-442 (2012).
59. J. C. Sluimer *et al.*, Hypoxia, hypoxia-inducible transcription factor, and macrophages in human atherosclerotic plaques are correlated with intraplaque angiogenesis. *J Am Coll Cardiol* **51**, 1258-1265 (2008).
60. I. Perrotta, The use of electron microscopy for the detection of autophagy in human atherosclerosis. *Micron* **50**, 7-13 (2013).

61. J. Magné *et al.*, ATG16L1 Expression in Carotid Atherosclerotic Plaques Is Associated With Plaque Vulnerability. *Arteriosclerosis, Thrombosis, and Vascular Biology* **35**, 1226-1235 (2015).
62. I. Nishino *et al.*, Primary LAMP-2 deficiency causes X-linked vacuolar cardiomyopathy and myopathy (Danon disease). *Nature* **406**, 906-910 (2000).
63. D. Klarin *et al.*, Genetics of blood lipids among ~300,000 multi-ethnic participants of the Million Veteran Program. *Nat Genet* **50**, 1514-1523 (2018).
64. T. G. Richardson *et al.*, Evaluating the relationship between circulating lipoprotein lipids and apolipoproteins with risk of coronary heart disease: A multivariable Mendelian randomisation analysis. *PLoS Med* **17**, e1003062 (2020).
65. I. Sergin *et al.*, Inclusion bodies enriched for p62 and polyubiquitinated proteins in macrophages protect against atherosclerosis. *Sci Signal* **9**, ra2 (2016).
66. I. Sergin *et al.*, Exploiting macrophage autophagy-lysosomal biogenesis as a therapy for atherosclerosis. *Nat Commun* **8**, 15750 (2017).
67. H. Koga, M. Martinez-Vicente, F. Macian, V. V. Verkhusha, A. M. Cuervo, A photoconvertible fluorescent reporter to track chaperone-mediated autophagy. *Nat Commun* **2**, 386 (2011).
68. M. Bourdenx *et al.*, Chaperone-mediated autophagy prevents collapse of the neuronal metastable proteome. *Cell* **184**, 2696-2714 e2625 (2021).

## Legend to the Figures

### Figure 1. CMA deficiency aggravates atherosclerosis in a murine experimental model.

(A-E) CMA activity in aorta from KFERQ-Dendra2 mice untreated (Control, A-C) or subjected to a pro-atherosclerotic treatment (injected with AAV8 PCSK9 and maintained for 12 weeks on Western-type diet, WD, D,E). Representative images of aorta sections co-stained with LAMP1 to highlight endolysosomal compartments. Insets: boxed areas at higher magnification. Arrows: fluorescent puncta. In C, animals were injected with fluorescent Dextran (in red) to highlight endolysosomal compartments. Individual and merged channels of the boxed region at higher magnification are shown. Arrows: Dextran+Dendra+ puncta (yellow) and Dextran+ only puncta (red). Collagen (red) was visualized by second harmonic generation in E. (F) Levels of LAMP-2A at the indicated times of the pro-atherosclerotic intervention. Representative images of aorta sections (left) and quantification in the neointima (right). n=18. (G-J) Circulating lipids in wild type (WT) and LAMP-2A null mice (L2AKO) subjected to the pro-atherosclerotic challenge for 12 weeks. Circulating total cholesterol (G), triglycerides (TG) (H), cholesterol profile (I) and TG profile (J). Individual values (G, H) and average curves (I, J) shown. n=13. (K-R) Plaque properties in the same mouse groups. Representative images of aortas stained for H&E (K) or sirius red (O) and quantification of plaque area (L), size of the necrotic core (M), plaque stage index (N), sirius red positive area (P) and cap thickness (Q). Calcification analysis in aortas stained for alizarin red (R) as shown in Supplementary Figure 11. n=16. (S,T) Representative images of aortas immunostained for  $\alpha$ SMA+ (VSMC) (S) and CD68 macrophages (T) and quantification of stained area (right) n=16. Individual values (symbols) and mean  $\pm$  SEM are shown. Experiments in panels A-E, were repeated 3 times with similar results. All data were tested for normal distribution using D'Agostino and Pearson normality test. Variables that did not pass normality test were subsequently analyzed using Mann-Whitney rank-sum test. All other variables were tested with the Student's t-test. \*p <0.05, \*\* p <0.01, \*\*\* p <0.005 and \*\*\*\* p <0.0001.

### Figure 2. A pro-atherogenic challenge elicits metabolic dysfunction in CMA deficient mice.

(A-E) Wild type (WT) and LAMP-2A null mice (L2AKO) subjected to a pro-atherosclerotic treatment (injected with AAV8 PCSK9 and maintained for 12 weeks on the Western-type diet, WD) were compared for body weight gain (n=14 WT, 16 L2AKO) (A), body composition (n=4) (Body composition: two-way ANOVA, F = 120.1; P < 0.0001 for interaction, F = 1736; P < 0.0001 for LEAN/FAT, F = 0.01544; P = 0.9032 for genotype, n = 4) (B), food intake (n=14 WT, 16 L2AKO) (C), energy expenditure (two-way ANOVA, F = 0.1185; P = 0.8889 for interaction, F = 21.05; P < 0.0001 for light/dark/total, F = 22.41; P = 0.0002 for genotype, n = 4) (D) and ambulatory parameters (x+z axis) (Ambulatory parameters: two-way ANOVA, F = 3.194; P = 0.0650 for interaction, F = 49.75; P < 0.0001 for light/dark /total, F = 20.75; P = 0.0002 for genotype, n = 4) (E). (F-I) Circulating levels in the same mouse groups of insulin (n=14 WT, 16 L2AKO) (F), glucose during an insulin tolerance test (repeated measures two-way ANOVA after Bonferroni's post hoc test, F = 1.851; P = 0.1090 for interaction, F = 31.96; P < 0.0001 for time, F = 15.99; P = 0.0040 for genotype, n = 4) (G), area under the curve from the insulin tolerance test (H) and circulating PAI-1 levels (n=14 WT, 16 L2AKO) (I). (J-M) Correlation between plasma cholesterol and different plaque parameters: plaque area (J), collagen (K), macrophages (L) and VSMC % of plaque area (M) in the same mouse groups (n=14 WT, 16 L2AKO). All data, when applicable, were tested for normal distribution using D'Agostino and Pearson normality test. Variables that did not pass normality test were subsequently analyzed using Mann-Whitney rank-sum test. All other variables were tested with the Student's t-test. Individual values (symbols) and mean  $\pm$  SEM are shown. \*p <0.05, \*\*p <0.01 and \*\*\*\*p <0.001.

**Figure 3. CMA blockage makes VSMC vulnerable to lipotoxicity and promotes their dedifferentiation.** (A) CMA activity in VSMC cells stably expressing the KFERQ-PS-Dendra2 CMA reporter and exposed to increasing concentrations of LDL. Representative images (left) of red channel (top) or merge channels (bottom). Nuclei were highlighted with DAPI. Quantification of CMA activity as the average number of fluorescent puncta per cell using high content microscopy ( $n > 2,500$  cells per condition in 6 different wells and 3 independent experiments). Statistically significant differences compared with basal (\*), or between groups with LDL (#), were analyzed by one-way ANOVA with Tukey's post-hoc test (\*\* $P < 0.005$ , \*\* $P < 0.005$ , \*\*\* $P = 0.001$ , \*\*\*\* $P < 0.001$  and # $P < 0.05$ ). (B) Intracellular levels of diLDL-derived fluorescence in VSMC from wild type (WT) and LAMP-2A null mice (L2AKO). Representative images (left) and quantification (right) ( $n = 3$ ,  $> 45$  cells per experiment in 3 different experiments). Inset: higher magnification. (C) Cytotoxicity in the same cells in response to increasing concentrations of LDL (two-way ANOVA after Bonferroni's post hoc test,  $F = 2.862$ ;  $P = 0.9872$  for interaction;  $F = 2.205$ ;  $P = 0.1570$  for LDL concentration,  $F = 21.93$ ;  $P = 0.0002$  for genotype,  $n = 5$ ). (D) Changes in mRNA levels of different markers of cell identity, macrophage-related and cholesterol pathway in the same VSMC stimulated with LDL or maintained in a LPDS (CTRL) (pool of 3 individual experiments). (E) STRING analysis for pathways differentially regulated in L2AKO cells in response to LDL compared to control (pool of 3 individual experiments). (F,G) Representative images (F) and quantification (G) of immunofluorescence for pYH2A.X in WT and L2AKO primary VSMC after LDL loading ( $n = 3$ ,  $> 5$  cells per experiment). (H) Immunoblot for components of the p53 signaling pathway in WT and L2AKO (L2A<sup>-/-</sup>) VSMC in basal conditions and upon LDL loading. Ponceau red staining is shown as loading control. The experiment was repeated 4 times with similar results. (I) BrDU incorporation in WT and L2AKO primary VSMC in basal conditions and upon LDL loading (two-way ANOVA after Bonferroni's post hoc test,  $F = 0.0002639$ ;  $P = 0.0183$  for interaction;  $F = 19.35$ ;  $P < 0.0001$  for cells with/without LDL,  $F = 19.61$ ;  $P < 0.0001$  for genotype,  $n = 4-5$ ). (J) Immunoblot (left) for HMGB1 in the culture media of WT and L2AKO primary VSMC in basal conditions and upon LDL loading. Quantification (right) (in arbitrary densitometric units (A.D.U.) of the indicated molecular weight variants of HMGB1 (26 kDa: two-way ANOVA after Bonferroni's post hoc test,  $F = 0.1301$ ;  $P = 0.7246$  for interaction;  $F = 2.801$ ;  $P = 0.1201$  for cells with/without LDL,  $F = 27.50$ ;  $P = 0.0002$  for genotype; 130 kDa: two-way ANOVA after Bonferroni's post hoc test,  $F = 2.578$ ;  $P = 0.1343$  for interaction;  $F = 2.516$ ;  $P = 0.1387$  for cells with/without LDL,  $F = 23.19$ ;  $P = 0.0004$  for genotype; 260 kDa: two-way ANOVA after Bonferroni's post hoc test,  $F = 0.2109$ ;  $P = 0.6543$  for interaction;  $F = 0.1635$ ;  $P = 0.6930$  for cells with/without LDL,  $F = 6.462$ ;  $P = 0.0258$  for genotype;  $n = 4-5$ ). (K) Changes in mRNA levels of main collagen genes in primary WT and L2AKO VSMC stimulated with LDL or maintained in a LPDS (CTRL) (pool of 3 individual experiments). All data, when applicable, were tested for normal distribution using D'Agostino and Pearson normality test. Variables that did not pass normality test were subsequently analyzed using Mann-Whitney rank-sum test. All other variables were tested with the Student's t-test. Values are mean  $\pm$  SEM. \* $p < 0.05$ , \*\* $p < 0.01$ , \*\*\* $p < 0.005$  and \*\*\*\* $p < 0.001$ .

**Figure 4. CMA blockage leads to exacerbated pro-inflammatory phenotype in macrophages.** (A,B) Levels of iNOS and COX-2 proteins in BMDM from wild type (WT) and LAMP-2A null mice (L2AKO) cultured without additions (control, CTRL) or stimulated with IFN $\gamma$ /LPS. Representative immunoblot (A) and densitometric quantification (B) expressed as folds over WT levels ( $n=5$  for iNOS and 3 for COX2). Ponceau red is shown as loading control. (C) mRNA levels of iNOS and Cox2 in the same cells expressed as folds over untreated (CTR). ( $n=4$ ). (D-J) Comparative proteomic analysis of lysosomes isolated from untreated (none) or leupeptin treated WT and L2AKO BMDM untreated (CTRL) or exposed to IFN $\gamma$ /LPS from a pool of 3 individual experiments. Schematic of the experimental design and anticipated results for hypothetical proteins undergoing CMA-dependent or -independent lysosomal degradation (D).

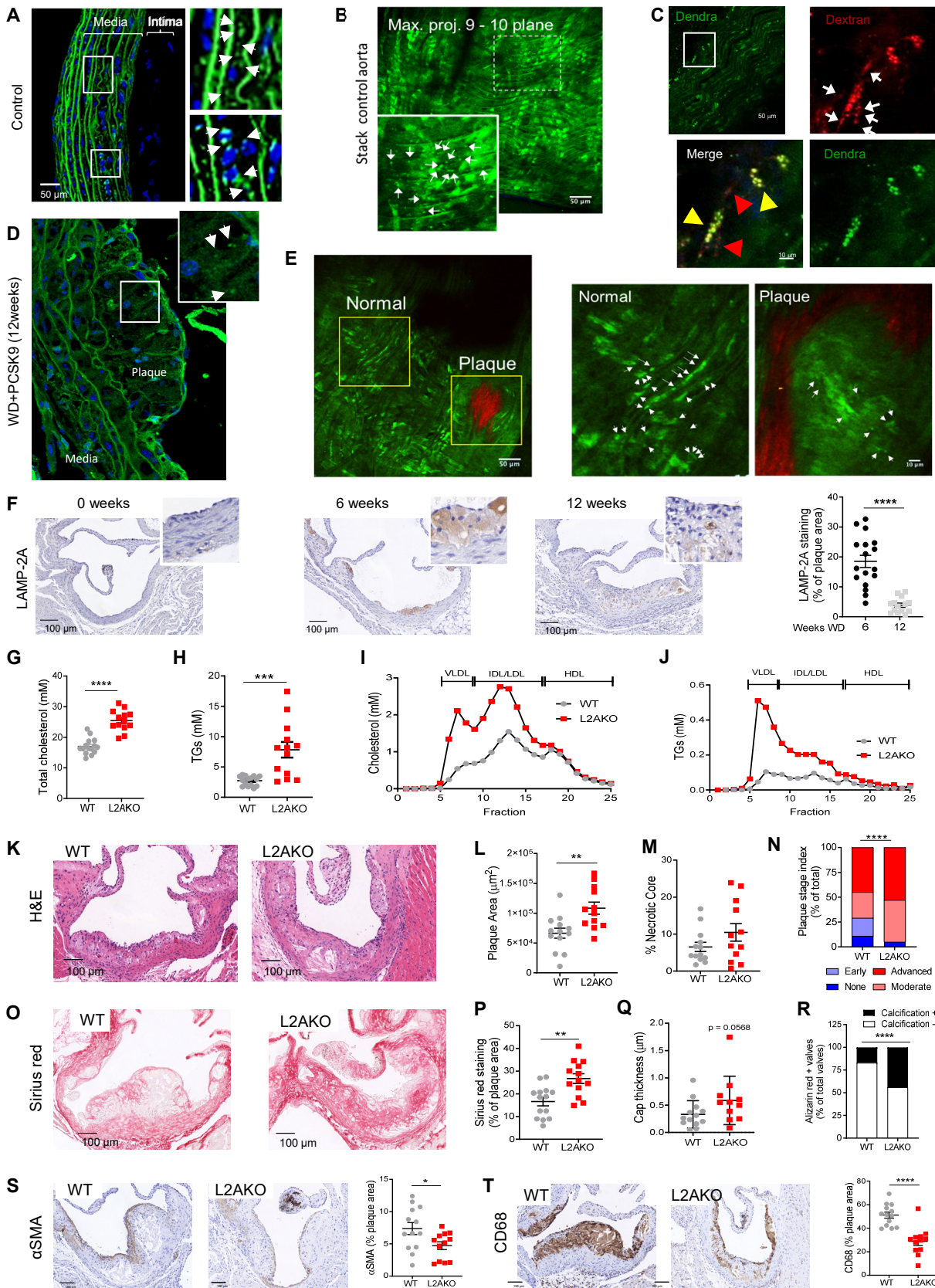
Percentage of lysosomal (constituents) and non-lysosomal proteins (substrates) in the fractions from CTRL and IFN $\gamma$ /LPS macrophages (E). Number (F) and percentage (G) of proteins undergoing lysosomal degradation (Total) in LAMP-2A dependent (CMA) or independent (no CMA) manner. STRING analysis for top intracellular networks of CMA substrates in CTRL (H) and IFN $\gamma$ /LPS (J) BMDM. Detail of changes in degradation of proteins involved in synthesis of nitric oxide (I), blue circle indicates proteins no longer degraded in lysosomes in the L2AKO group and down arrows the reduction in lysosomal degradation of those proteins in the same group. (K-N) Number of total monocytes (K), pro-inflammatory subtype of monocytes (L), total T cells (M) and TCD4 cells (N) in WT and L2AKO mice (n=14 WT and n=16 L2AKO). All data, when applicable, were tested for normal distribution using D'Agostino and Pearson normality test. Variables that did not pass normality test were subsequently analyzed using Mann-Whitney rank-sum test. All other variables were tested with the Student's t-test. All values are mean  $\pm$  SEM. Individual values are shown also in i-l. \*p <0.05, \*\*p <0.01, \*\*\*p <0.005 and \*\*\*\*p <0.001.

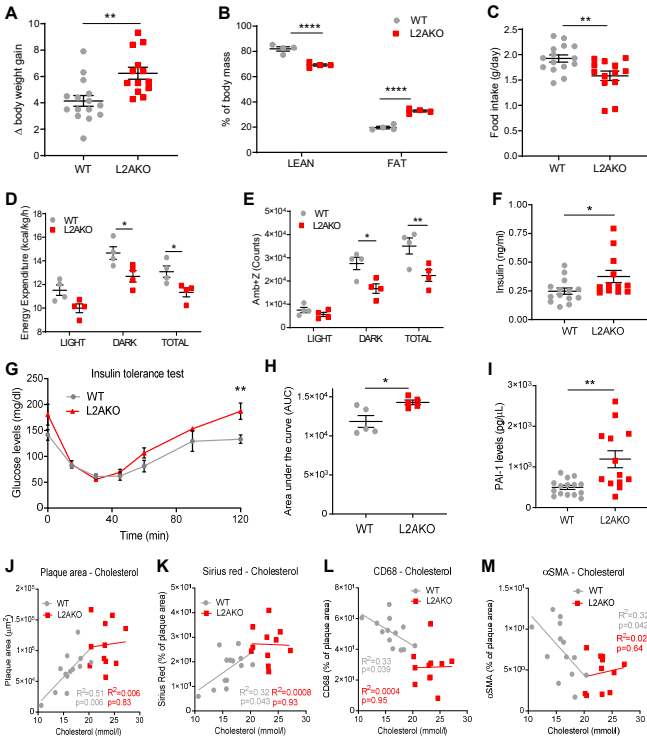
**Figure 5. CMA changes in aorta of atherosclerotic patients with disease.** (A-G) LAMP-2A levels in different stages of carotid artery atherosclerotic plaque development sourced from asymptomatic subjects at autopsy (study 1). Representative images of the colocalization of LAMP-2A with  $\alpha$ SMA (A) and CD68 (B) positive cells in human atherosclerotic plaques. Representative images of H&E staining (left) and LAMP-2A immunostaining (middle, and higher magnification on right) (C), quantification of LAMP-2A staining intensity relative to plaque area (D). Correlation between mRNA levels of LAMP-2A and plaque area (E) and extent of the necrotic core (F) in carotid artery plaques from symptomatic subjects (study 2). Comparison of immunostaining for LAMP-2A (middle) and the macrophage marker CD68 (right) in adjacent sections from the same patient (G, study 1) and correlation between the mRNA levels of LAMP-2A and macrophage content (H, study 2). All stains were performed in 35 human samples with an average age of 65.8 years for the patients with one event and 72.8 years for the patients with a secondary event (study 1). (I) Normalized expression (within each cell type) of individual component of the CMA network in scRNAseq from human coronary atherosclerotic plaques from heart transplants (study 3). Only three major cell types are highlighted here, results for the other cell types can be found in Figure S6B. CMA network elements are organized in functional groups and colored dots indicate the effect of a given element on CMA activity (Green: positive element; Red: negative element). (J,K) Protein levels for LAMP2 and Cathepsin D in carotid artery plaque lysates from symptomatic patients who experienced a secondary coronary event (2ary event) or not (no 2ary event) (study 4, n = 21/group) subjected to immunoblot. Average and individual values in all samples independent of gender (J) and representative immunoblot (top) and values in females only (K). Ponceau red is shown as loading control. (L,M) CMA activation score (L) calculated from normalized mRNA expression data (shown in M) between stable and unstable carotid artery atherosclerotic plaques (study 2). Decrease of the score indicates a predicted transcriptional inhibition of the pathway [t41=1.612, p=0.1146]. Normalized expression of individual component of the CMA network in RNAseq from stable and unstable atherosclerotic plaques (study 2). CMA network elements are organized in functional groups and colored dots are as in I. All data, when applicable, were tested for normal distribution using D'Agostino and Pearson normality test. Variables that did not pass normality test were subsequently analyzed using Mann-Whitney rank-sum test. All other variables were tested with the Student's t-test. Individual patient values and mean  $\pm$  SEM are shown. \*p <0.05 and \*\*p <0.01. n=36 for the first study. n=15-20 for the second study.

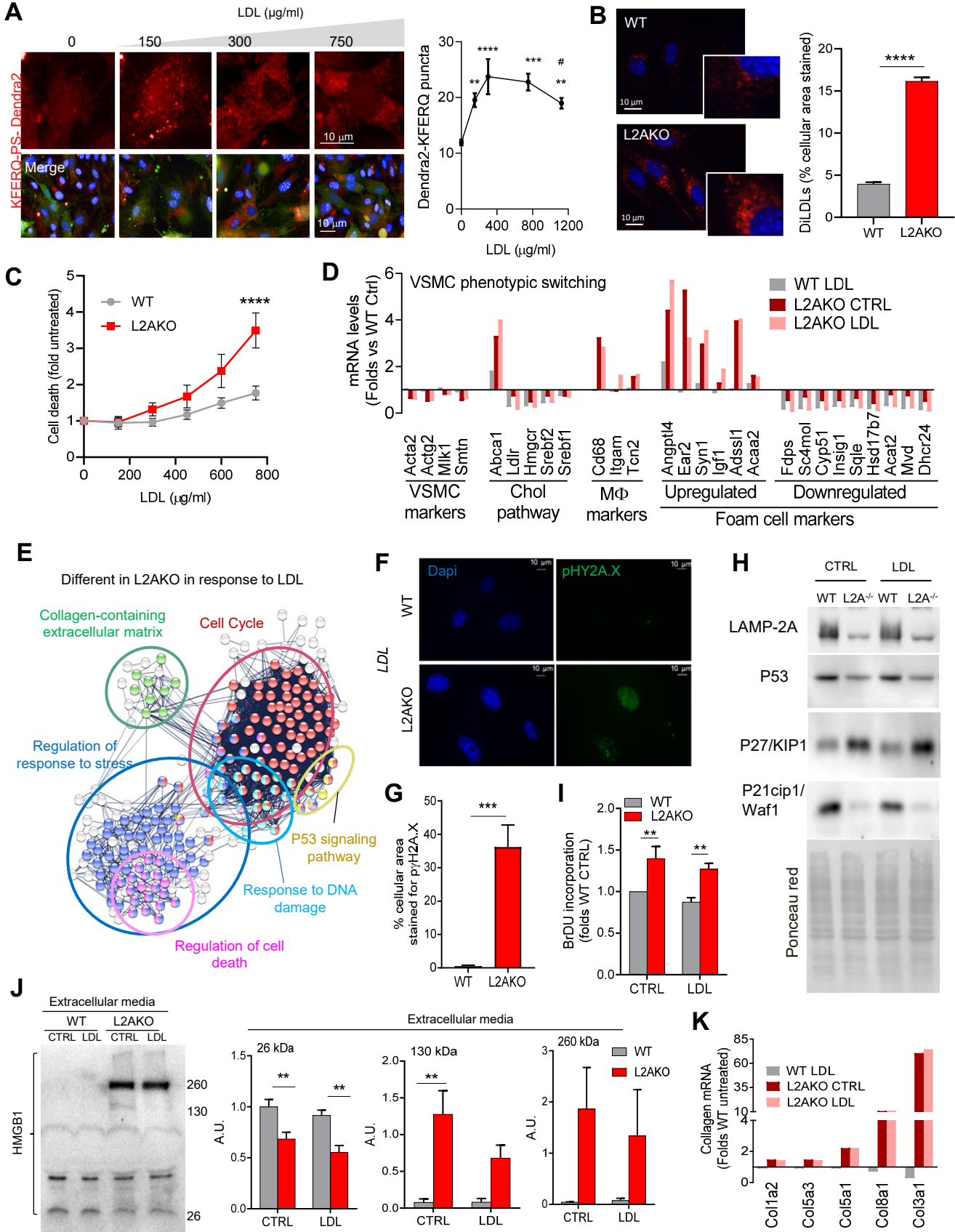


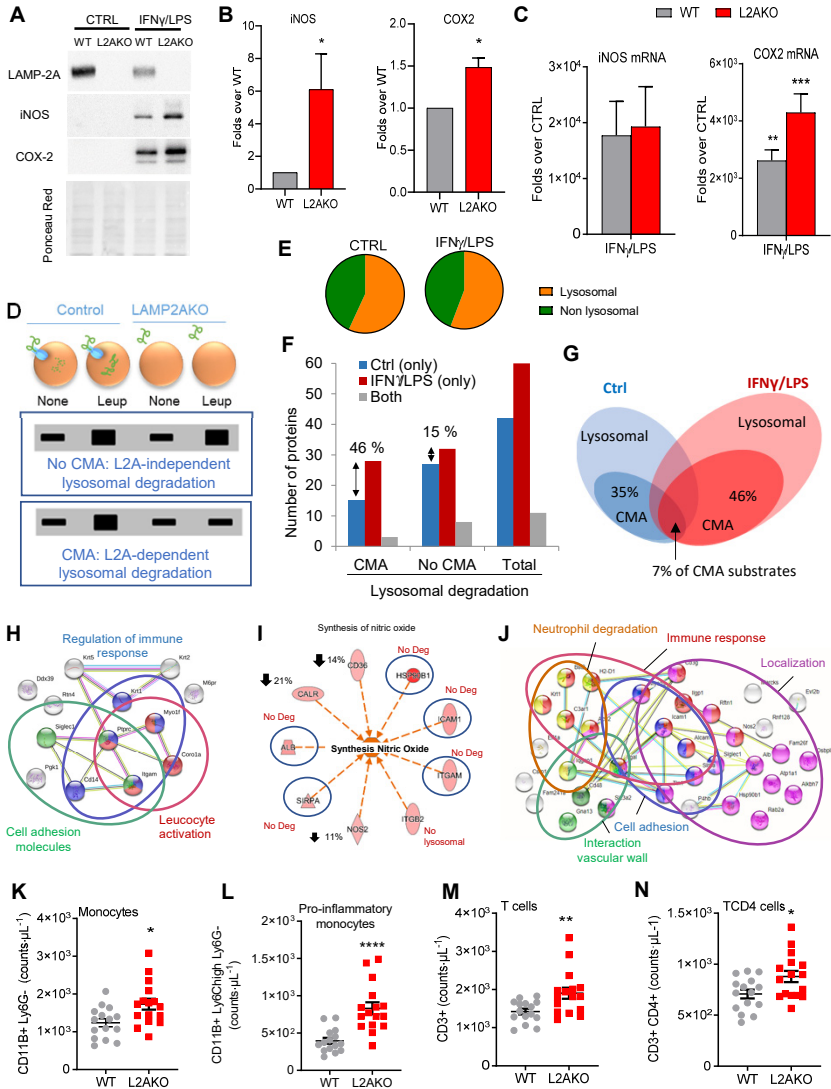
**Figure 6. Genetic upregulation of CMA ameliorates disease in an atherosclerosis murine experimental model.** (A-D) Circulating lipids in control mice (CTRL) and in mice systemically expressing a copy of human LAMP-2A (hL2AOE) subjected to a pro-atherosclerotic intervention (injected with AAV8 PCSK9 and maintained for 12 weeks on the Western-type diet). Circulating total cholesterol (A), triglycerides (TG) (B), cholesterol profile (C) and TG profile (D). n=9 CTRL, n=8 hL2AOE. (E) Insulin tolerance test in the same mice (repeated measures two-way ANOVA after Bonferroni's post hoc test, F = 3.159; P = 0.0047 for interaction, F = 21.02; P < 0.0001 for time, F = 1.578; P = 0.098 for genotype) in the same mice. (F-L) Properties of the plaques from aortas of the same mouse groups. Representative images of aortas stained for H&E (F), Alizarin red (I) or sirius red (K) and quantification of plaque area (G), size of the necrotic core (H), calcification presence (J) and collagen deposition (L). n=9 CTRL, n=8 hL2AOE. (M,N) Principal component analysis of 12 variables measured in CTRL and hL2AOE mice. Each dot represents a single animal (M). Ellipses are the 95% confidence interval around the center of mass of a given experimental group. Bar plot represents mean +/- s.e.m. of PC1 score for each experimental group (N). n=9 CTRL, n=8 hL2AOE. \*: Student t-test between CTRL and hL2AOE t15=2.152, p=0.048. Individual values and mean ± SEM are presented in all quantifications. All data were tested for normal distribution using D'Agostino and Pearson normality test. Variables that did not pass normality test were subsequently analyzed using Mann–Whitney rank-sum test. All other variables were tested with the Student's t-test. \*\*p <0.01.

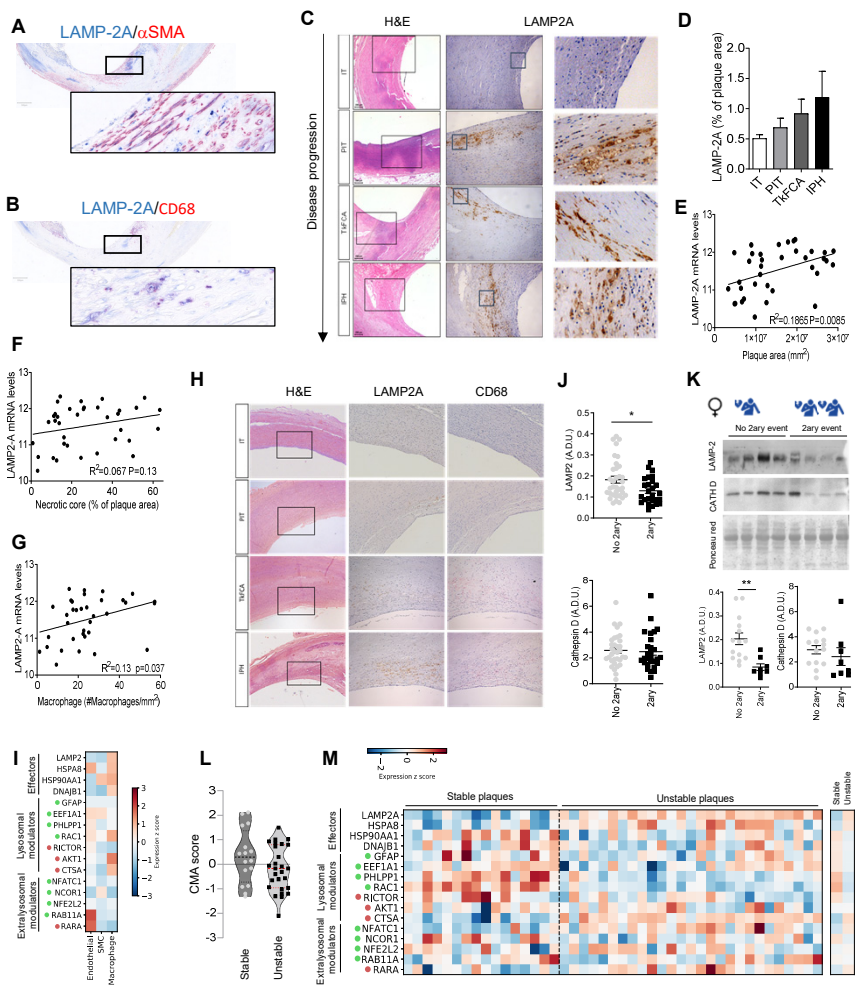
**Figure 7. CMA is part of the systemic and vascular response against pro-atherosclerotic insults.** The protective effect of CMA against atherosclerosis results from the combination of systemic and vasculature-specific functions of CMA. Left: systemic CMA failure leads to defective lipid and glucose metabolism that increases systemic vulnerability to the metabolic syndrome. Right: Defective CMA in vascular smooth cells makes them prone to dedifferentiation because of failure to degrade proteins involved in cellular proliferation, collagen secretion and cell death. Macrophages unable to upregulate CMA in response to a lipotoxic stimuli acquire a more proinflammatory phenotype with higher NO levels, increased migratory capability and defective LPS metabolism.



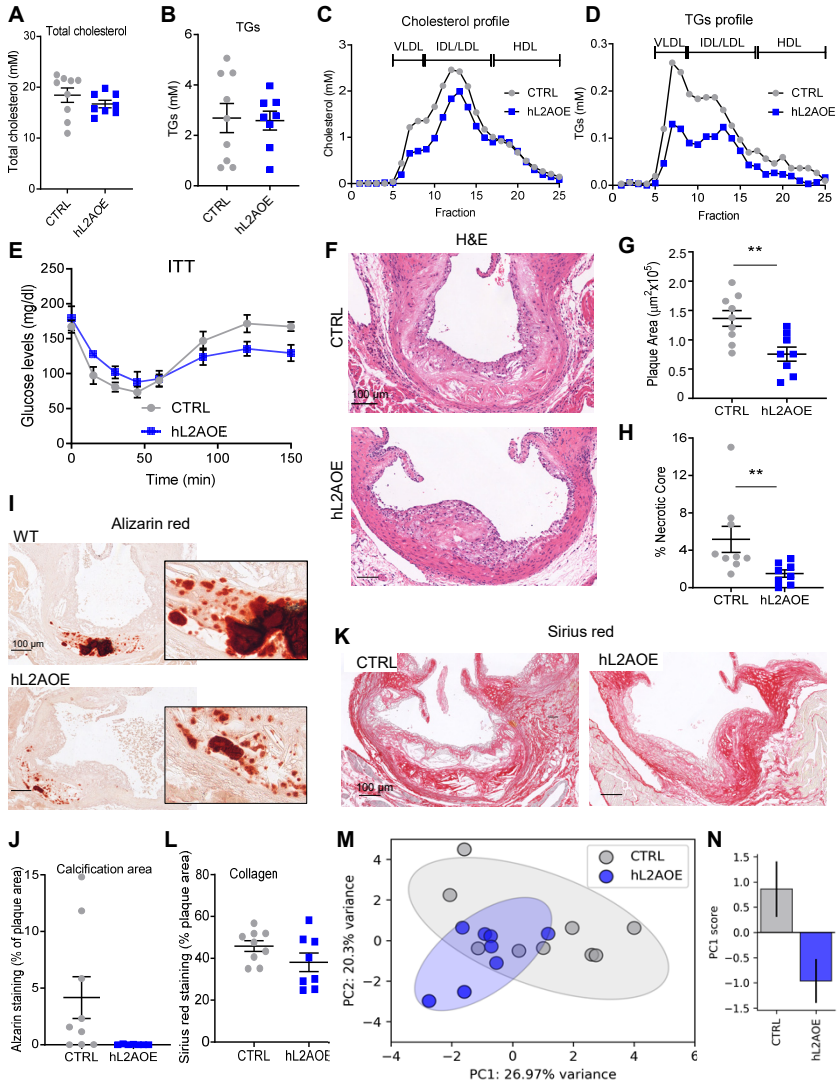




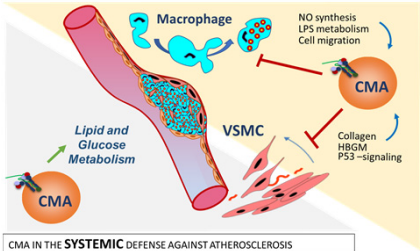








CMA IN THE **CELL-INTRINSIC** DEFENSE AGAINST ATHEROSCLEROSIS





## **Supplementary Information for** Protective role of chaperone-mediated autophagy against atherosclerosis

Julio Madrigal-Matute<sup>a,b</sup>, Jenny de Bruijn<sup>c</sup>, Kim van Kuijk<sup>c</sup>, Dario F Riascos-Bernal<sup>d</sup>, Antonio Diaz<sup>a,b</sup>, Inmaculada Tasset<sup>a,b</sup>, Adrián Martín-Segura<sup>a,b</sup>, Marion J.J. Gijbel<sup>c,e</sup>, Bianca Sander<sup>c</sup>, Susmita Kaushik<sup>a,b</sup>, Erik A.L. Biessen<sup>c</sup>, Simoni Tiano<sup>a,b</sup>, Mathieu Bourdenx<sup>a,b</sup>, Gregory J. Krause<sup>a,b</sup>, Ian McCracken<sup>f</sup>, Andrew Baker<sup>f</sup>, Han Jin<sup>c</sup>, Nicholas Sibinga<sup>a,d</sup>, Jose Javier Bravo-Cordero<sup>g</sup>, Fernando Macian<sup>h</sup>, Rajat Singh<sup>a,b,d</sup>, Patrick C.N. Rensen<sup>i</sup>, Jimmy F.P. Berbée<sup>j†</sup>, Gerard Pasterkamp<sup>k</sup>, Judith C. Sluimer<sup>c,f,1</sup>, Ana Maria Cuervo<sup>a,b,d,1</sup>.

<sup>1</sup>To whom correspondence may be addressed: Ana Maria Cuervo MD PhD, [ana-maria.cuervo@einsteinmed.edu](mailto:ana-maria.cuervo@einsteinmed.edu) and Judith Sluimer PhD, [judith.sluimer@maastrichtuniversity.nl](mailto:judith.sluimer@maastrichtuniversity.nl)

### **This PDF file includes:**

Supplementary text  
Figures S1 to S7  
Tables S1 to S6  
SI References

### **Other supplementary materials for this manuscript include the following:**

Dataset S1

## Supplementary Information Text

### Extended Methods

#### Animal models and treatments

KFERQ-PS-Dendra2 mice (1) were generated by donor egg injection in wild type FVB mice using the pRP.ExSi plasmid backbone with the insert coding for 11 amino acids including the KFERQ sequence of RNase A in frame with the sequence of Dendra2 under the hybrid promoter CAGG and crossed back more than 9 generations to C57BL/6J. Male C57BL/6J LAMP-2A knock-out (L2AKO) were generated as described before (2). C57BL/6J mice conditionally expressing hLAMP-2A (hL2AOE) (3) were generated by inserting the hLAMP-2A cDNA sequence with a STOP cassette (a neo cassette flanked by two Loxp sites) into mouse ROSA26 locus in PTL1 (129B6 hybrid) ES cells that were used to generate heterozygous mice carrying the ROSA26-STOP-hLAMP-2A allele. Crossing these mice with  $T^{mx}ER$ -Cre mice generated a mouse line in which expression of hLAMP-2A could be induced by injection of tamoxifen (TMX) (4 intraperitoneal (i.p.) injections of 20 mg/kg b.w. on alternate days). Male mice (KFERQ-PS-Dendra2, WT, L2AKO, CTRL and hL2AOE) were intraorbitally injected at 12 weeks of age with a single dose of AAV8-PCSK9 ( $1.0 \times 10^{11}$ VC) to promote the degradation of LDLR and increase circulating cholesterol levels (4). Atherosclerosis was further induced by feeding the mice a Western-type diet (WD; D12108; ResearchDiets; saturated fats (35 kcal%), cholesterol (1.25% w/w) and cholic acid (0.22% w/w)) for 12 weeks. KFERQ-PS-Dendra2, WT and L2AKO mice were fed a WD for 12 weeks and sacrificed for further analysis. After 6 weeks on diet, when we observed the drop in CMA activity, CTRL and hL2AOE were injected with TMX to activate expression of hLAMP-2A and all mice were monitored for 10 additional weeks (3). This longer protocol was required to compensate for the reduced intestinal absorption of cholesterol observed in the first 2 weeks upon TMX injection (5). For leupeptin treatment, mice were i.p. injected with leupeptin (30 mg/kg b.w.; Sigma, L5793) or PBS single injection 12h and 2h before euthanizing. Mice were all in the C57BL/6J background and housed in ventilated cages with no more than 5 mice per cage on a 12h light/dark cycle at 23°C with free access to water and food in the institutional barrier facility along with sentinel cages and were specific pathogen-free. Genotyping, breeding and treatments in this study were done accordingly to protocol and all animal studies were under an animal study protocol approved by the Institutional Animal Care and Use Committee of Albert Einstein College of Medicine.

#### Primary cell cultures, cell lines and treatments

VSMC were isolated from 8 weeks old mice aortas (pool of 5 mice per genotype) by collagenase digestion and maintained in DMEM (Gibco) supplemented with 20% fetal bovine serum (FBS, Gibco), 2mM L-glutamine, 100 U/ml penicillin and 100 µg/ml streptomycin (Invitrogen). LPDS was prepared from FBS delipidated with 4% fumed silica (6). VSMC were incubated for 24h in DMEM media plus 5% LPDS with or without LDL (150 µg/ml LDL-cholesterol) plus 0.1 U/ml of bovine lipoprotein lipase (7). For Dil-LDL production, LDL was labeled with the fluorescent probe Dil (Invitrogen) as previously described (8).

Bone marrow derived macrophages (BMDM) were isolated from 8 weeks old mice and differentiated in non-treated tissue culture plates by using Iscove's Modified Dulbecco's medium (IMDM) containing 20% of FBS and supplemented with 20% of L-929 cells conditioned media. After 5 days in culture, nonadherent cells were eliminated and adherent cells were trypsinized and seeded into the final plates for treatment (6). Macrophage stimulation was attained by removing the culture medium and culturing cells for an additional 18h in DMEM supplemented with 5% FBS (for CTRL) or 5% FBS, 20 ng/ml IFN- $\gamma$ , and 100 ng/ml LPS (for IFN- $\gamma$ /LPS) (9).

#### Human samples

Tissue samples and human mRNA and RNAseq data included in this study are from 4 different cohorts as follows (see also **Tables S2** and **S3**).

Study 1: Human carotid plaque samples (n=38, mean age 72 years, 64% men) representing the following stages of atherosclerosis: intimal thickening, pathological intimal thickening, thick fibrous cap (stable) atheroma, and plaque with intraplaque hemorrhage, were obtained anonymously at autopsy from subjects without cardiovascular symptoms and no additional clinical information was collected. Collection, storage and use of tissues were performed

in agreement with the Dutch Code for Proper Secondary use of Human Tissue. An opt-out arrangement was in place at time of hospital admission, and hence tissues were not used in case of objection by relatives in line with the guidelines provided by the Dutch Code for Proper Secondary use of Human Tissue. None of the co-authors were directly involved with tissue collection.

**Study 2:** mRNA expression by microarray analysis was obtained from previously published studies (10). Briefly, atherosclerotic plaque samples were obtained during carotid endarterectomy (n=24 symptomatic patients, mean age 72.9 years, age range 64-83 years, 100% men, clinical characteristics in Supplementary Table 1 of (10)). All experiments were conducted in agreement with the code for proper secondary use of human tissue in the Netherlands (<http://www.fmwv.nl>). This study complies with the Declaration of Helsinki, and the local Medical Ethical Committee in accordance with national regulations approved use of this tissue (protocol number 16-4-181 and O3-114O). Plaques were segmented for histology, and flanked segments used for RNA isolation. Classification of all used plaques was performed on H&E-stained slides according to Virmani *et al* (11), by experienced cardiovascular pathologists (JCS, MG). Plaques with and without intraplaque hemorrhage were compared. No follow-up is available.

**Study 3:** Single cell RNAseq data was obtained from previously published studies (12). Briefly, human coronary arteries dissected from explanted hearts of transplant recipients were obtained from the Human Biorepository Tissue Research Bank under the Department of Cardiothoracic Surgery from consenting patients, with approval from the Stanford University Institutional Review Board (n=4, ages 65, 54, 65 and 58 years, 100% men, clinical characteristics in Supplementary Table 4 of (12)). Histology is not available.

**Study 4:** Human atherosclerotic plaques were from the AtheroExpress Study biobank, in which plaques from patients undergoing carotid endarterectomy were obtained and segmented for serial histology or snap frozen for protein/RNA isolation. Patients were included if they suffered a symptomatic ischemic event within 6 months prior to the surgery. Plaques were segmented for histology and adjacent protein isolation. After surgery, patients were followed up for a minimum of three years to assess if they underwent a secondary major adverse cardiovascular event or not. Subjects with one event at baseline were compared with subjects who also had a second event at follow-up (n= 40, mean age 69.9, age range 58-83 years, 100% men, clinical characteristics per group shown in **Table S3**).

In the analysis of aortas from individuals of different ages RNAseq data was obtained from the GTEx portal (13) (<https://gtexportal.org> (dbGaP Study Accession: phs000424.v8.p2) and single cell RNAseq data was from the Tabula Sapiens (14) (<https://tabula-sapiens-portal.ds.czbiohub.org/>). Details of these studies are summarized in **Table S2**).

### **Antibodies**

Primary antibodies were from the following sources (dilutions, commercial source and catalog number indicated in brackets): rat anti-LAMP2 (1/500, Hybridoma Bank, GL2A7), rabbit anti-LAMP-2A (1/5000, Thermo Scientific, 512200), rabbit anti-LDLr (1/1000, Abcam, ab52818), rabbit anti-human LAMP-2A (1/1000, Abcam, ab18528), rat anti-LAMP1 (1/500, Hybridoma Bank, 1D4B), mouse anti-human LAMP2 (1/500, Hybridoma Bank, H4B4), rabbit anti-LC3 (1/1000, Cell Signaling, 2775), rabbit anti-P62 (Enzo Life Sciences BMLPW98600100), mouse anti- $\beta$ -actin (1/10000 Sigma, A4700), anti-CD68 (rat, 1/200 Bio-Rad, mca1957; rabbit, ab125212, Abcam), anti- $\alpha$ -SMA (rabbit, 1/500 Abcam, ab202510; mouse, F3777, Sigma; mouse, M0851, Dako), goat anti-Cathepsin D (1/500, Santa Cruz, sc-6486), mouse IgM anti-HSC70 (1/5000, Novus Biologicals, nb120-2788), rabbit anti-iNOS (1/1000, Cell Signaling 2977), rabbit anti-COX-2 (1/1000, Cell Signaling, 12282), mouse anti-p53 (1/1000, Cell Signaling, 2524), rabbit anti-P27 (1/1000, Cell Signaling, 2552), rabbit, anti-P21 (1/1000, Abcam, ab109199) and anti-HMGB1 (1/1000, Abcam, ab18256). All the secondary antibodies were from Thermo Scientific. All antibodies used in this study were from commercial sources and were validated following the multiple dilution method and, where available, using cell lines or tissues from animals knock-out for the antigen. Sources of chemicals were as described before (2, 15).

### **Tissue dissection and Histological Procedures**

All mice were euthanized with a pentobarbital overdose (100 mg/kg i.p.) and blood was withdrawn via the right ventricle for flow cytometry and biochemical analysis. Mice were perfused via the left cardiac ventricle with PBS containing sodium nitroprusside (0.1 mg/ml; Millipore). Aortic arch and

organs of interest were dissected and fixed in 1% PFA overnight and paraffin-embedded. Aortic roots were serially sectioned and stained with hematoxylin and eosin (H&E) for plaque area and necrotic core content. Five consecutive H&E sections at 20 µm intervals were analyzed blindly using computerized morphometry (Leica QWin V3) and averaged per mouse. A 100 µm interval where a fully developed media within the aortic valves was present was determined for each mouse. Sections within this 100 µm interval were used for immunohistochemical staining. Plaques were staged as early (intimal xanthoma), moderate (pathologic intimal thickening, PIT), or advanced (fibrous cap atheroma) as described before (16). Two sections per mouse were stained with Sirius Red for collagen quantification and averaged per mouse. Immunostaining for LAMP-2A in mouse aorta was performed using a rabbit anti-LAMP-2A (Thermo scientific; 512200) following standard procedures. Macrophages and VSMC were immunostained using rabbit anti-CD68 (ab125212, Abcam) antibody followed by secondary anti-rabbit HRP-labeled antibody (DPVR-55-HRP, Immunologic) and anti-αSMA (F3777, Sigma) followed by secondary-HRP-labelled antibody (11.426.346.910, Roche), respectively. Epitope-antibody binding was visualized as a brown precipitate using diaminobenzidine. Alizarin red (A5533-25G, Sigma) was used to detect calcification. For colocalization staining, primary antibodies, followed by secondary anti-rabbit AP-labelled antibody (DPVR-55-AP, Immunologic) were used in CD68 and LAMP-2A staining, and for VSMC staining mouse anti-αSMA (M0851, Dako) primary antibody, followed by secondary anti-mouse Biotin-labelled antibody (RPN1001v1, Amersham) and ABC-AP amplification (AK-5000, Vector) were used. Epitope-antibody binding was visualized as either blue or red precipitate using Vector substrate kits (SK-5300 or SK-51000, respectively).

#### **Lipid analysis**

Plasma was obtained by centrifugation at 6,000g for 10 min at 4°C, snap-frozen and stored at -80°C until further use. Pooled plasma samples from mice according to genotype and treatment were used for lipoprotein fractionation on a Superose 6 PC 3.2/30 column (ÄKta System, Amersham Pharmacia Biotech). The samples were eluted at a constant flow rate of 50 µl/min in PBS (pH 7.4). Fractions of 50 µl were collected and assayed for TC and TG using the kits described above. Plasma levels of insulin and PAI-1 were measured using ELISA (90080, Crystal Chemicals and ab197752, Abcam). Plasma levels of CCL3, CCL4 and G-CSF were measured using MILLIPLEX MAP Mouse Cytokine/Chemokine kit (Millipore) in a Luminex Magpix (Luminex).

#### **Metabolic analysis**

Body weight was measured weekly during the study period. Body composition was determined on 21-week-old mice by magnetic resonance spectroscopy (MRS) using an echo MRS instrument (Echo Medical System) and metabolic measurements (oxygen consumption, carbon dioxide production, food intake, and locomotor activity) were obtained continuously every 8 minutes using a CLAMS (Columbus Instruments) open-circuit indirect calorimetry system for 8 days. Insulin resistance was measured with an intraperitoneal insulin tolerance test (ITT) performed on 21-week-old mice after 4h fasting. Blood glucose was measured before i.p. of insulin (1.5 U/kg body weight) and then 15, 30, 45, 60, 90, 120 and 150 minutes after injection.

#### **Flow cytometry and serum parameters**

Whole blood cell composition was analyzed using flow cytometry after erythrocyte lysis and incubation with the following specific antibodies to detect leucocyte subsets: leucocytes (CD45+; 103129, Biolegend), T cells (CD3ε+, NK1-1-; 48-0032-80, ThermoFisher), T helper cells (CD4+; 15-0041-81, ThermoFisher), cytotoxic T cells (CD8a+; 11-0081-82, ThermoFisher), B cells (CD45R/B220+; 561227, BD), NK cells (NK1-1+; 561046, BD), granulocytes (CD11bhigh Ly6Ghigh; 11-0112-41 ThermoFisher, 560600, BD, respectively) and monocytes (CD11bhigh Ly6Glow Ly6Chigh/intermediate/low) using the Absolute Counting Tubes (340334, BD Trucount). Data were acquired using a Becton Dickinson LSRII-U and analyzed with FACSDiva software (BD) and gating strategy is depicted in **Supplementary Scheme 1**.

#### **Human carotid plaque analysis**

Human carotid autopsy samples (study 1) were processed for immunohistochemistry as follows. After antigen retrieval (target retrieval DAKO), slides were incubated overnight with primary antibody (Human LAMP-2A (ab18528, Abcam), CD68 (macrophage marker, ab125212, Abcam) or αSMA (VSMC marker, F3777, Sigma)), followed by secondary-biotin-labelled antibodies, and ABC-

HP amplification (Vector). Epitope-antibody binding was visualized as a brown precipitate using diaminobenzidine. Colocalization of LAMP-2A and CD68 and  $\alpha$ SMA was done on directly adjacent sections using rabbit anti-LAMP-2A (18528, Abcam), mouse anti-CD68 (M0814, Dako) and mouse anti- $\alpha$ SMA (M0851, Dako) primary antibodies respectively, followed by either anti-mouse or anti-rabbit AP-labelled secondary antibody (DPVM-55-AP or DPVR-55-AP, Immunologic). Epitope-antibody binding was visualized as either a blue (LAMP-2A) or red (CD68/ $\alpha$ SMA) precipitation using Vector substrate kits (SK-5300 or SK-51000 respectively).

LAMP-2A mRNA expression in thick fibrous cap atheromas and intraplaque hemorrhage-rich plaques was analyzed by microarray derived from paired segments of the same patient undergoing carotid endarterectomy (study 2) (10). LAMP-2A mRNA expression intensities from microarrays were correlated with morphometrically analyzed histological plaque characteristics: plaque size, necrotic core (% of plaque) and macrophages (% CD68 of plaque).

LAMP-2 protein expression in human atherosclerotic plaque was analyzed using the AtheroExpress Study biobank, in which plaques from patients undergoing carotid endarterectomy were obtained (study 4). Protein lysates of these plaques were used for western blot analysis and compared between groups with one event at baseline or a second event at follow up.

### **CMA activity**

CMA activity *in vivo* was determined in aorta arches from KFERQ-Dendra2 mice using CT embedding method as following: Aortas were fixed for 12h at 4°C in fixation buffer (2% formaldehyde, 0.2% picric acid in PBS, pH7.0) and then washed with 70% ethanol, followed by two washes in PBS. Tissues were immersed in 30% sucrose and then embedded in OCT for sectioning in a cryostat (Leica CM3050 S). After air-drying for 30 min, sections were stored at -20°C until use. Colocalization of LAMP1, CD68 and  $\alpha$ SMA was done on sequential serial sections using rat anti-LAMP-1 (Hybridoma Bank, 1D4B), rat anti-CD68 (Bio-Rad, mca1957) and rabbit anti- $\alpha$ SMA (Abcam, ab202510, alexa 594-labelled). Slices were mounted in DAPI-Fluoromount-G to highlight the cell nucleus. Direct fluorescence images were obtained with a confocal microscope (TCS SP5; Leica) using an HCX Plan Apo CS 63.0 $\times$  1.40 NA oil objective in the Leica Application Suite X (LAS X) or an Olympus FV1000 multiphoton microscope with a 25 $\times$  1.05 NA water immersion objective as previously described(17). Collagen was visualized by second harmonic generation.

CMA activity in cultured VSMC was measured using lentivirus-mediated expression of fluorescent photoswitchable KFERQ-PSDendra2 reporter (18). Cells were photoswitched with a 405nm light emitting diode (LED: Norlux) for 3 min with 3.5mA (constant current) and 16 h later fixed with 1% paraformaldehyde. Images were acquired with an Axiovert 200 fluorescence microscope (Carl Zeiss), with 1.4 numerical aperture. The average number of fluorescent puncta per cell was quantified using Image J (NIH) in individual single planar images after thresholding. Values are presented as number of puncta per cell section that in our acquisition conditions represents 10-20% of the total puncta per cell (19).

### **Lysosomal isolation**

Lysosomes were isolated from BMDM after disruption of the plasma membrane by nitrogen cavitation and sequential centrifugation in Percoll/metrizamide discontinuous density gradients (20). Preparations with more than 10% broken lysosomes, measured by  $\beta$ -hexosaminidase latency, were discarded (20).

### **Microarray**

Total RNA from a pool of 3 independent experiments with VSMC in culture was extracted using TRIzol (Invitrogen) and purified with RNeasy chromatography (Qiagen) in LPDS media and LPDS plus LDL (150  $\mu$ g/ml). Cy3-labeled RNA (0.6  $\mu$ g) from each condition were hybridized to Agilent Mouse 8x60K. Data were processed using the oligo package and normalized using Robust Multiarray Average (RMA) method. Gene set was filtered to remove genes without Entrez or GO annotation (21912 genes out of 55682) and genes with an IQR > 0.5. The full microarray raw data has been deposited in GEO accession number GSE49553. Pathway analysis was performed using the IPA software (Ingenuity Systems) and STRING database (<https://string-db.org/>).

### **Calculation of CMA score**

Expression intensities (log) for every gene in the CMA network were preprocessed and normalized as described (21). First, to avoid dimensionality issue, each gene was centered and scaled across

all patients. Then, for every patient (or cell type in scRNAseq data), a CMA score was calculated by computing an eigengene, which is a weighted average expression over all genes in the corresponding CMA network. To do so, each element of the CMA network (22) was attributed a *weight*. As LAMP-2A is the rate limiting component of CMA, it was given a *weight* of 2. Every other element received a *weight* of 1. Then, every element was attributed *direction* score that is +1 or -1 based on the known effect of a given element on CMA activity (21). The score was then calculated as the weighted/directed average of expression counts of every element of the CMA network. Higher scores, predictive of CMA activation, could result from (i) increased expression of effectors or positive modulators or (ii) decreased expression of negative modulators. Conversely, (i) decreased expression of effectors or positive modulators, or (ii) a higher expression of negative modulators will render lower CMA activation scores. CMA score calculation and plotting was done using Python (Python software foundation v.3.7.4 available at <https://www.python.org/>) and the scientific python stack: scipy (v.1.3.1), numpy (v.1.17.2), and matplotlib (v.3.1.1).

### **Quantitative Proteomics and Protein Pathway Analysis**

BMDM lysosomes active for CMA were isolated from WT and L2AKO macrophages treated in CTRL or stimulated with IFN $\gamma$ /LPS and treated or not (untreated) with 2 mM NH $_4$ Cl and 100  $\mu$ M leupeptin 12 hours before isolation. Lysosomes from three different sets were pooled and analyzed for purity, integrity, ponceau red electrophoretic patterning and enrichment in markers of CMA lysosomes by immunoblot. Quantitative proteomics analysis was performed in the two different genotypes under the four different conditions using isobaric tags for relative and absolute quantitation (iTRAQ) by Applied Biomics, Inc.. For each sample (10  $\mu$ g of protein), the buffer was replaced with 0.5 M triethylammonium bicarbonate, pH 8.5, followed by reduction, alkylation, trypsin digestion, iTRAQ labeling, and sample clean-up according to the manufacturer's instructions (AB SCIEX). NanoLC was carried out using a Dionex Ultimate 3000 (Milford, MA). Tryptic peptides were loaded into a  $\mu$ -Precolumn Cartridge and separated on an acetonitrile gradient (ranging from 5% to 60%) on a C18 Nano LC column. Fractions were collected at 20-second intervals followed by Mass Spectrometry analysis on AB SCIEX TOF/TOF<sup>TM</sup> 5800 System (AB SCIEX). Mass spectra were acquired in reflectron positive ion mode. TOF/TOF tandem MS fragmentation spectra were acquired for each ion, averaging 4,000 laser shots per fragmentation spectrum on (excluding trypsin autolytic peptides and other known background ions). The resulting fragmentation spectra were submitted to MASCOT search engine (version 2.3, Matrix Science) to search the database of National Center for Biotechnology Information non-redundant (NCBI nr). Searches were performed without constraining protein molecular weight or isoelectric point, with variable methyl-thiolation of cysteine and oxidation of methionine residues, fixed N-terminal- and lysine-modifications with iTRAQ labels, and one missed cleavage. Quantitation was performed on peptides displaying an ion score confidence interval of 95 percent or higher.

For each protein hit the average ratio(s) for the protein, the number of peptide ratios that contributed, and the geometric standard deviation were determined. Values in the L2AKO untreated experimental groups were compared to their respective NH $_4$ Cl/leupeptin treated samples and then with their respective WT groups and are represented as the average of folds (lysosomes isolated from untreated WT BMDM are given a value of 1). CMA substrate proteins were defined as those for which leupeptin treatment resulted in increase in lysosomal levels >10% and with a reduction in NH $_4$ Cl/leupeptin response of >10% in the L2AKO. Validation of the subset of proteins of interest was performed by immunoblotting in lysosomal fractions isolated from independent BMDM (not shown). The protein sets catalogued as CMA substrates from the iTRAQ experiments were analyzed using the IPA software (Ingenuity Systems) and STRING database (<https://string-db.org/>).

### **Real-Time Quantitative-Polymerase Chain Reaction**

Total RNA was isolated from cells using TRIzol Reagent (Invitrogen). RNA (1  $\mu$ g) was used to perform the reverse transcription with High Capacity cDNA Archive Kit (Applied Biosystems). Real-time PCR reactions were performed on an ABI Prism 7500 sequence detection PCR system (Applied Biosystems) according to manufacturer's protocol, using the  $\Delta\Delta$ Ct method as described (23). Quantification of mRNA levels was done by amplification of cDNA using Power SYBR Green PCR Master Mix (4368702, ThermoFisher). The primer sequences are listed in **Table S6**. Expression levels are given as ratio to housekeeping gene HPRT1 and data is expressed as fold

vs basal values.

### **Other methods**

Rates of cellular proliferation were determined as incorporation of BrdU 24h after plating (11444611001, Sigma) and cytotoxicity was determined by ApoTox-Glo Triplex Assay (G6320, Promega). Electrophoresis and immunoblot were performed using nitrocellulose membranes after cell lysis in 0.25M sucrose buffer (pH 7.2) containing protease and phosphatase inhibitors. Cell lysates were centrifuged at increasing speeds to discard intact cells (300 g, 10 min) and dead cells (2,000 g, 10 min). After electrophoresis and transfer to nitrocellulose membrane, the proteins of interest were visualized by incubation of the membranes with the primary and corresponding secondary antibody by chemiluminescence using peroxidase-conjugated secondary antibodies in G-BOX Chemi XX6 (Imgen).  $\beta$ -actin and red ponceau were used as loading control. Macroautophagy was measured upon transduction of cells with a lentiviral vector expressing mCherry-GFP-LC3 (24), as the conversion of dual fluorescence puncta (autophagosomes) into only red fluorescent puncta (autolysosomes). Immunoblot for LC3 and P62/SQSTM1 in cells incubated for 12h with  $\text{NH}_4\text{Cl}$ /leupeptin was used to analyze macroautophagy flux.

### **Statistical analysis**

All data are presented as individual values (symbols) and/or mean+SEM For *in vitro* assays we determined the number of experimental repetitions to account for technical variability and changes in culture conditions. In all instances, “n” refers to individual experiments or animals. Data comes from a minimum of three independent experiments and instances with higher number of repetitions are indicated in the figure legends. The number of animals used per experiment was calculated through power analysis based in previous results. Animals were randomly attributed to control or treatment groups. No mouse was excluded from the analysis unless there were technical reasons, or the mouse was determined to be in very poor health by the veterinarian. Outliers were determined by the ROUT method (Q = 1%). Investigators were blinded to the treatment during data collection and analysis and unblinding was done when the analysis was completed for plotting. If not indicated otherwise, all parameters were analyzed using independent sample tests and were tested for normal distribution using Shapiro-Wilk normality test. Parameters with two groups were compared with student’s t-test or Mann-Whitney rank-sum test, depending on outcome of the D’Agostino & Pearson normality test. In case of more than two groups, parameters were analyzed using two-way ANOVA followed by Bonferroni’s Multiple Comparison Test or Kruskal-Wallis rank-sum test, followed by Dunn’s post-hoc testing, in the absence of a normal distribution. CMA activity measured by KFERQ-Dendra2 puncta in VSMC was subjected to Analysis of Variance (One-way ANOVA) followed by Tukey’s post hoc tests. Time course experiments were analyzed using repeated measured (mixed model) ANOVA, followed by Bonferroni post-tests upon confirmation of homogeneity of variances using Levene’s (GraphPad 7.0). Human plaque analysis. Correlation analysis was performed using Spearman bivariate correlation analysis (IBM SPSS statistics 22). Human plaque L2A levels were significantly skewed, thus square root transformation normalized the distribution. As L2A levels were significantly different between male and females, we performed sex-stratified logistic regression analysis of the association of the incidence of a second cardiovascular event with stepwise, forward inclusion (wald) of square-root transformed L2A, age, hypertension and BMI (n=22 females, 37 males). Also, the sex-stratified associations of square-root transformed L2A, age, hypertension and BMI with time to a second event were analysed using cox regression. Analysis was done with IBM SPSS statistics (version 25).

### **Materials availability**

All reagents generated in this study are available from the Lead Contact with a completed Material Transfer Agreement.

### **Data and code availability**

There are no restrictions on data availability in this manuscript. All the information is included in the manuscript. All Main and Supplementary Figures have associated raw data that is provided as an Excel worksheet organized by figures and it includes statistics along with exact p values. The full microarray raw data has been deposited in GEO accession number GSE49553. This manuscript does not report original code.



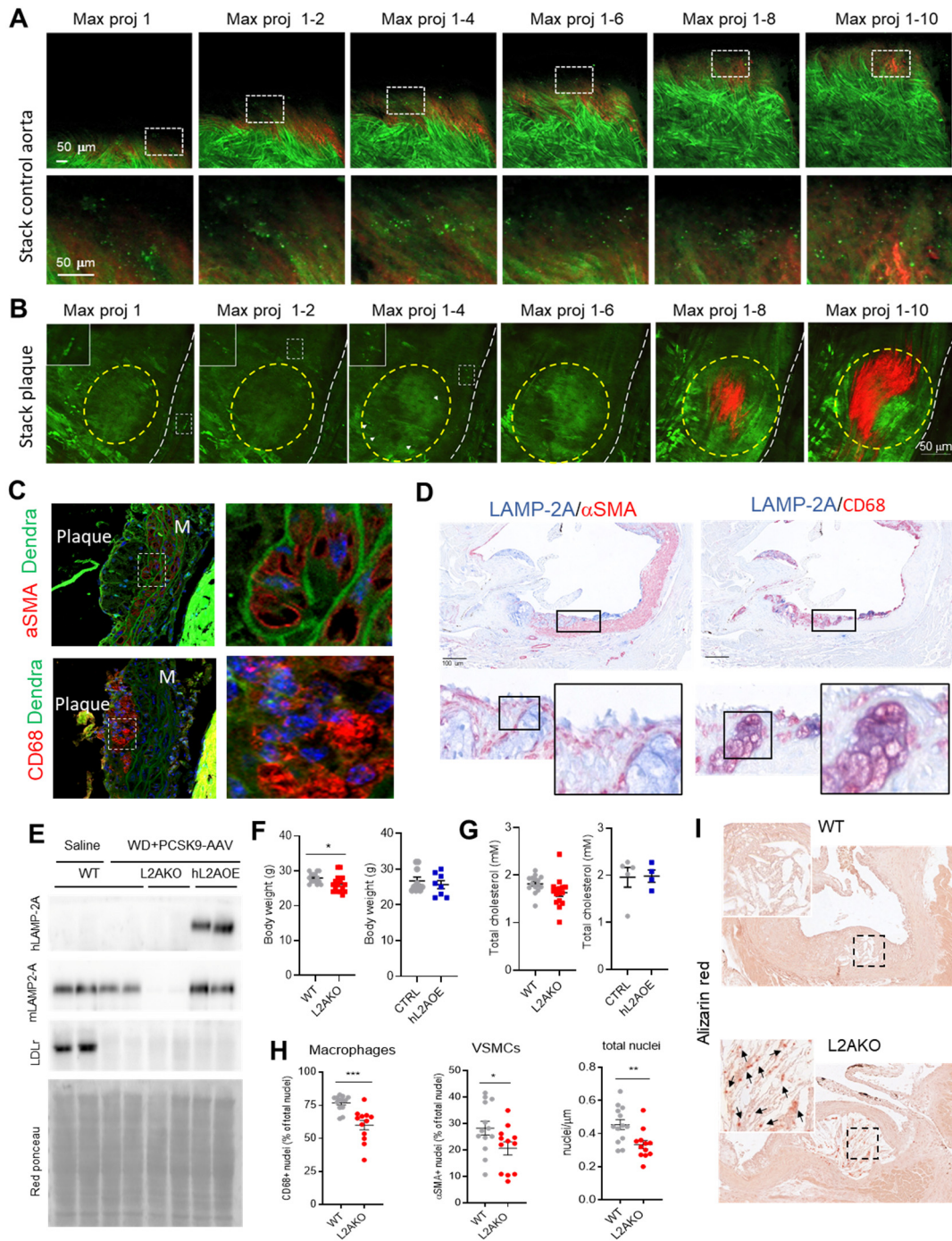


**Figure S1. Characterization of the mouse models used in this study.** (A,B) Representative images of aortas from KFERQ-Dendra2 mice untreated (Control, A) or subjected to a pro-atherosclerotic treatment (injected with AAV8 PCSK9 and maintained for 12 weeks on the Western-type diet) (B). Sequential maximal projections are shown. Insets show boxed area at higher magnification. In B the plaque region is denoted by the circle and identified by the accumulation of collagen (red). (C) Aorta sections containing atherosclerotic plaques from the KFERQ-Dendra2 mice in B, co-stained with  $\alpha$ -SMA or



CD68. Insets on right show boxed area at higher magnification. M: media. Experiments in A-C were repeated 3 times with similar results. (D) Representative images of the colocalization of LAMP-2A with  $\alpha$ SMA (left) and CD68 positive cells (right) in a murine atherosclerotic plaque. (E) Immunoblot for human LAMP-2A (hLAMP-2A), murine LAMP-2A (mLAMP-2A) and LDLR in livers from wild type (WT), LAMP-2A null mice (L2AKO) and mice systemically expressing a copy of human LAMP-2A (hL2AOE) injected retro-orbitally with saline or AAV8-PCSK9 as indicated. Ponceau red is shown as loading control. (F,G) Basal metabolic parameters in WT, L2AKO and hL2AOE mice at 3 months of age. Body weight (F) and total cholesterol levels (G). (n=15 CTR, n=16 L2AKO, n=9 hL2AOE). (H) Total number of nuclei (right) and percentage of macrophages (left) and VSMCs (middle) in plaques from wild type (WT) and LAMP-2A null mice (L2AKO) subjected to the pro-atherosclerotic challenge for 12 weeks. (I) Representative images of Alizarin red staining of aorta from WT and L2AKO mice subjected to the pro-atherosclerotic intervention. Insets: boxed area at higher magnification. Arrows: calcium deposits. Quantification is shown in Figure 1R. All data, when applicable, were tested for normal distribution using D'Agostino and Pearson normality test. Variables that did not pass normality test were subsequently analyzed using Mann–Whitney rank-sum test. All other variables were tested with the Student's t-test. Individual values (symbols) and mean  $\pm$  SEM are shown. \*p <0.05, \*\*p <0.01 and \*\*\*p<0.001.

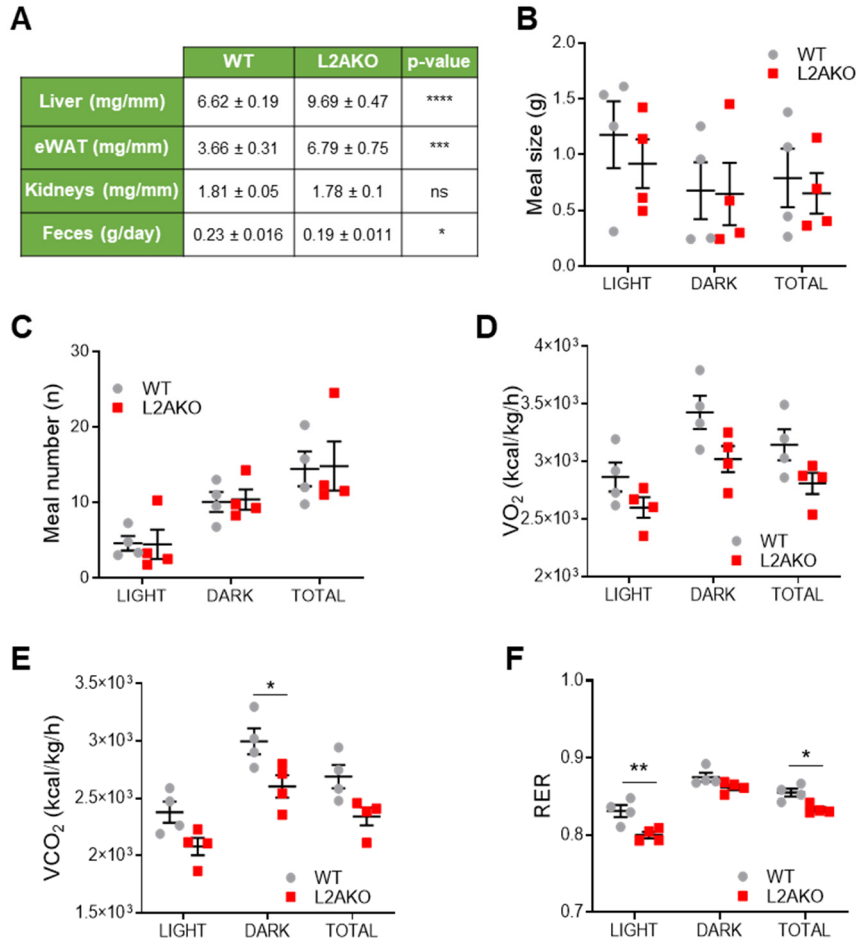


**Figure S2. Metabolic profile of CMA deficient mice subjected to an experimental model of murine atherosclerosis.** (A) Tissue weights after 12 weeks of Western-type diet ( $n = 15$ ) in wild-type (WT) and LAMP-2A null mice (L2AKO). Tissue weights are normalized by tibial length and expressed as mean  $\pm$  SEM. (B-F) Metabolic parameters measured by indirect calorimetry in WT and L2AKO mice fed a Western-type diet for 6 weeks: Meal size (Meal size: two-way ANOVA,  $F = 0.1027$ ;  $P = 0.9029$  for interaction,  $F = 1.359$ ;  $P = 0.2820$  for light/dark/ total,  $F = 0.4767$ ;  $P = 0.4987$  for genotype,  $n = 4$ ) (B), meal number (Meal number: two-way ANOVA,  $F = 0.01$ ;  $P = 0.99$  for interaction,  $F = 12.83$ ;  $P = 0.0003$  for light/dark/ total,  $F = 0.0122$ ;  $P = 0.9133$  for genotype,  $n = 4$ ) (C), volume of  $O_2$  consumption ambulatory parameters ( $VO_2$ : two-way ANOVA,  $F = 0.1759$ ;  $P = 0.8401$  for interaction,  $F = 8.587$ ;  $P = 0.0024$  for light/dark/total,  $F = 12.04$ ;  $P = 0.0027$  for genotype,  $n = 4$ ) (D), volume of  $CO_2$  production ( $VCO_2$ : two-way ANOVA,  $F = 0.1254$ ;  $P = 0.8829$  for interaction,  $F = 18.38$ ;  $P < 0.0001$  for light/dark/total,  $F = 20.33$ ;  $P = 0.0003$  for genotype,  $n = 4$ ) (E) and RER (RER: two-way ANOVA,  $F = 1.537$ ;  $P = 0.2419$  for interaction,  $F = 54.04$ ;  $P < 0.0001$  for light/dark/total,  $F = 27.8$ ;  $P < 0.0001$  for genotype,  $n = 4$ ) (F). All data were tested for normal distribution using D'Agostino and Pearson normality test. Variables that did not pass normality test were subsequently analyzed using Mann-Whitney rank-sum test. All other variables were tested with the Student's t-test. ns indicates p-value = non-significant. Graphs represent individual values, mean  $\pm$  SEM. \* $p < 0.05$  and \*\* $p < 0.01$ .

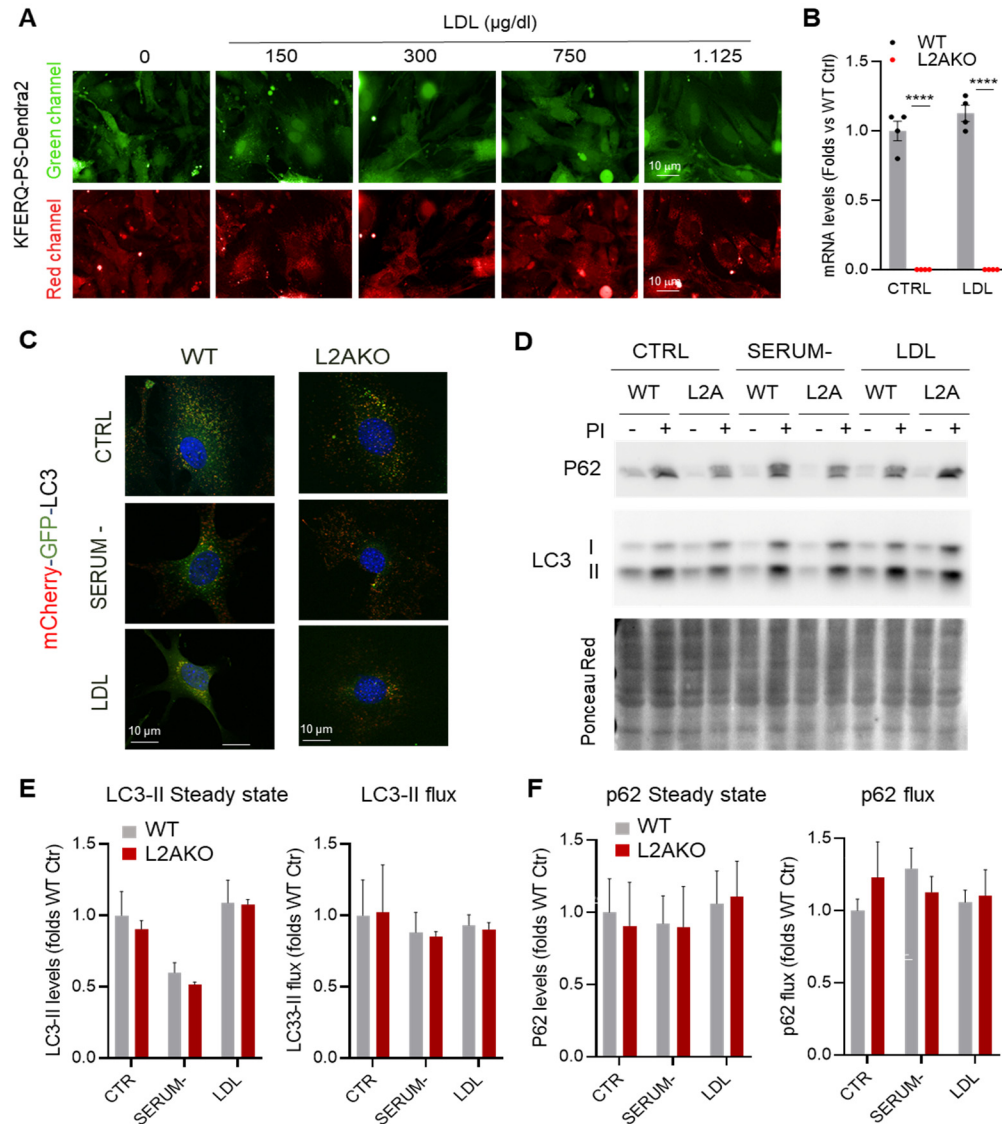


**Figure S3. Autophagic changes in VSMC upon lipid challenges.** (A) CMA activity in murine VSMC stably expressing the KFERQ-PS-Dendra2 CMA reporter and challenged with the indicated concentrations of LDL. Representative images of separate channels. Quantification is shown in Figure 3A. (B) LAMP-2A mRNA in VSMC cells isolated from WT and L2AKO mice and exposed to the indicated lipid challenge.  $n=4$  isolations from 4 independent mice per group. (C) Macroautophagy flux detected by direct fluorescence in WT and L2AKO VSMC transfected with the tandem reporter mCherry-GFP-LC3. Representative images of merged channels are shown. Nuclei are highlighted with DAPI. The experiment was repeated 4 times with similar results. (D-F) Macroautophagy flux detected by immunoblot for LC3-II and P62/SQSTM1 in WT and L2AKO VSMC under the indicated conditions, detected as an increase in LC3-II and p62 intensity upon inhibition of lysosomal hydrolysis with protease inhibitors (PI). Ponceau red was used as loading control. Quantification of steady state (left) and flux (right) for LC3-II (E) and p62 (F) from the densitometric analysis of blots as the ones shown in D. Values are mean+s.e.m. of 4 independent experiments. \*\*\*\* $p<0.001$

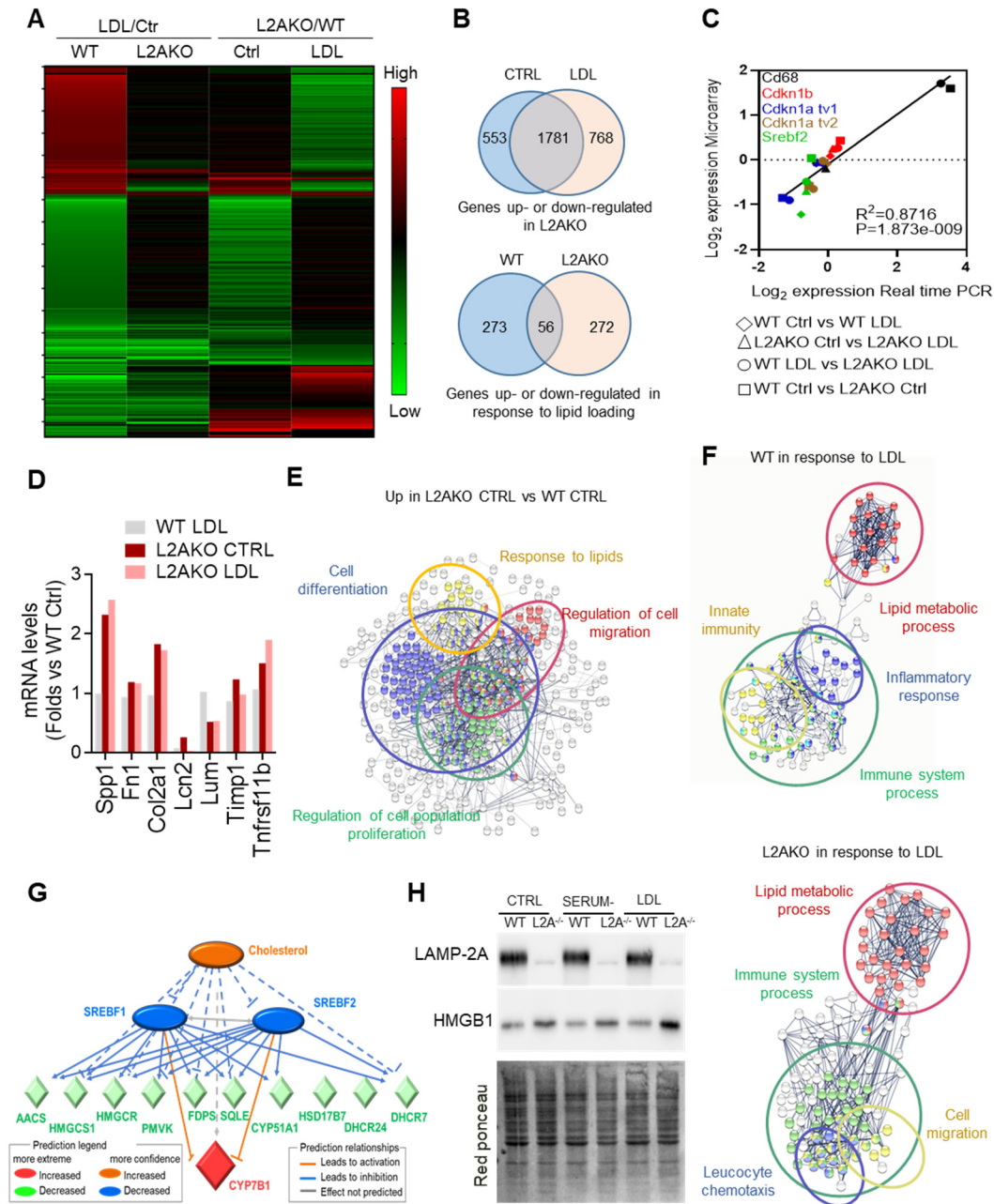


**Figure S4. Differential transcriptional and protein profile of CMA-deficient VSMC.** (A) Hierarchical heatmap of transcriptional changes (Log<sub>2</sub> fold) in VSMC from wild type (WT) and LAMP-2A null mice (L2AKO) cultured under basal conditions (control, CTRL) or upon LDL loading. (B) Venn diagrams showing the number of genes upregulated and downregulated (cutoff  $>\pm 1$  log<sub>2</sub> fold change) WT and L2AKO VSMC in basal conditions (top) or in response to LDL treatment (bottom) compared to the same conditions in the WT cells. (C) Validation by RT-PCR of selected genes identified in the microarray in three independent experiments and to *Hprt1* expression. Scatter plot showing the significant positive relationship between selected mRNA gene expression obtained by microarray and RT-PCR. Level of significance was determined by Pearson correlation.  $R^2=0.8716$ ;  $P=1.873e-09$ . (D) Changes in mRNA levels of genes recently identified as markers of

modified dedifferentiated VSMC (12) in primary WT and L2AKO VSMC stimulated with LDL or maintained in a LPDS (CTRL) (pool of 3 individual experiments). (E,F) STRING analysis for pathways upregulated in L2AKO cells under basal conditions (E) or changing in response to LDL loading (F) in WT (top) or L2AKO VSMC (bottom). (G) Cholesterol biosynthetic network identified as one of the top networks of genes modulated differentially in WT and L2AKO primary VSMC. Red: increase, green: decrease. (H) Representative immunoblot for HMGB1 in cellular lysates of WT and L2AKO primary VSMC maintained in basal conditions or upon serum removal (-) or LDL loading. The experiment was repeated 3 times with similar results. All GEO terms are significant for  $p < 0.01$ .

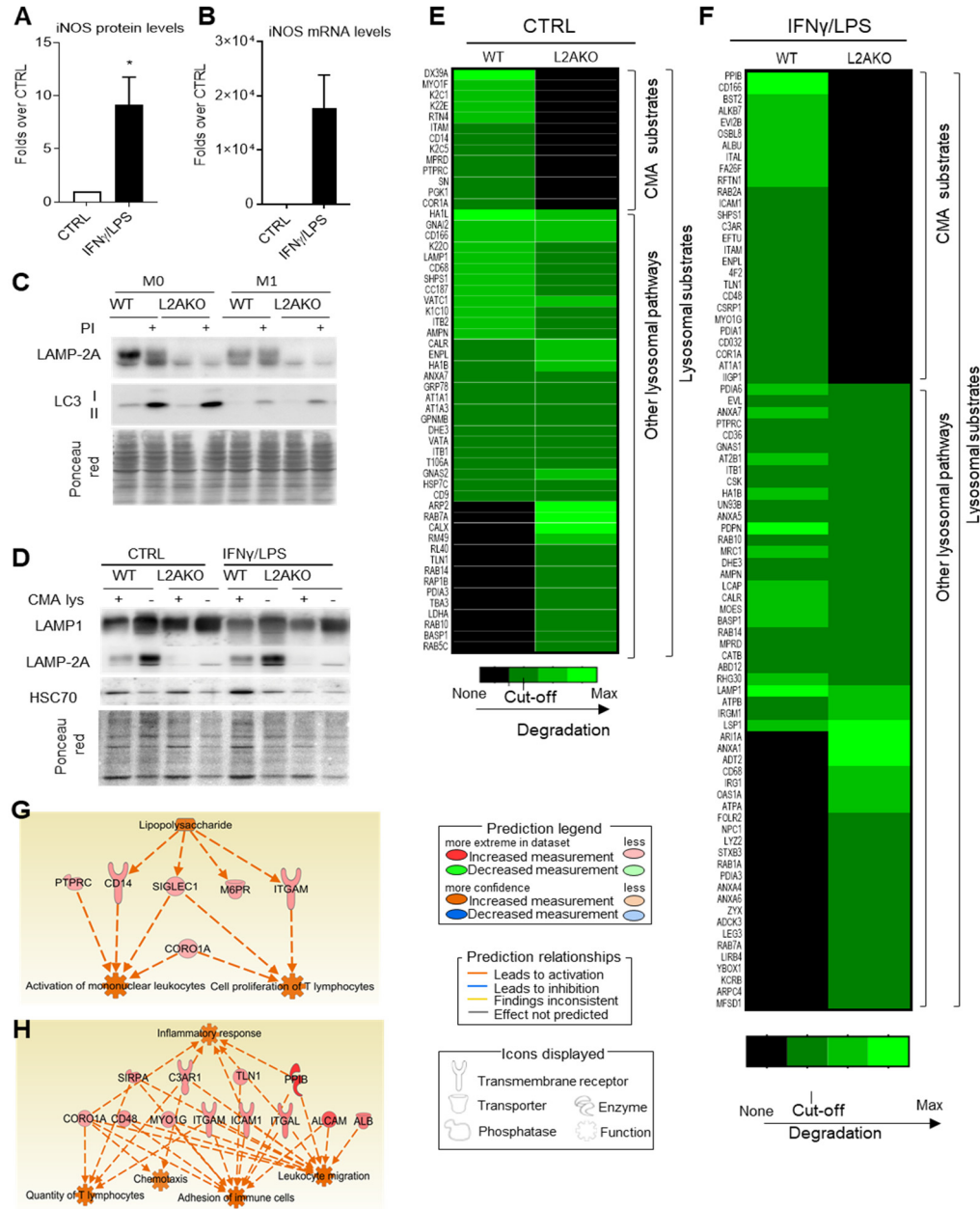


**Figure S5. Characterization of CMA-deficient macrophages.** (A,B) Levels of iNOS protein (A) and mRNA (B) in BMDM from wild type (WT) and LAMP-2A null mice (L2AKO) cultured without additions (control, CTRL) or stimulated with IFN $\gamma$ /LPS. n=4. (C) Macroautophagy flux detected by immunoblot for LC3-II in WT and L2AKO M0 and M1 BMDM, detected as an increase in LC3-II intensity upon inhibition of lysosomal hydrolysis with protease inhibitors (PI). Ponceau red was used as loading control. The experiment was repeated 2 times with similar results. (D) Representative immunoblot for the indicated lysosomal components (LAMP1, LAMP-2A and HSC70) in lysosomes with high (+) or low (-) activity for CMA isolated from WT or L2AKO mouse BMDM. Ponceau red is shown as loading control. The experiment was repeated 3 times with similar results. (E,F) Heat map of changes in levels of the proteome of lysosomes from WT or L2AKO mouse BMDM CTRL (E) or exposed to IFN $\gamma$ /LPS (F) upon inhibition of lysosomal proteolysis. (G,H)

Predicted activation in BMDM L2AKO cells of the LPS pathway due to accumulation of CMA substrates (G) and the inflammatory response in IFN $\gamma$ /LPS treated cells (H) using the IPA software. All data, when applicable, were tested for normal distribution using D'Agostino and Pearson normality test. Variables that did not pass normality test were subsequently analyzed using Mann–Whitney rank-sum test. All other variables were tested with the Student's t-test. Graphs represent mean  $\pm$  SEM. \*p <0.05.



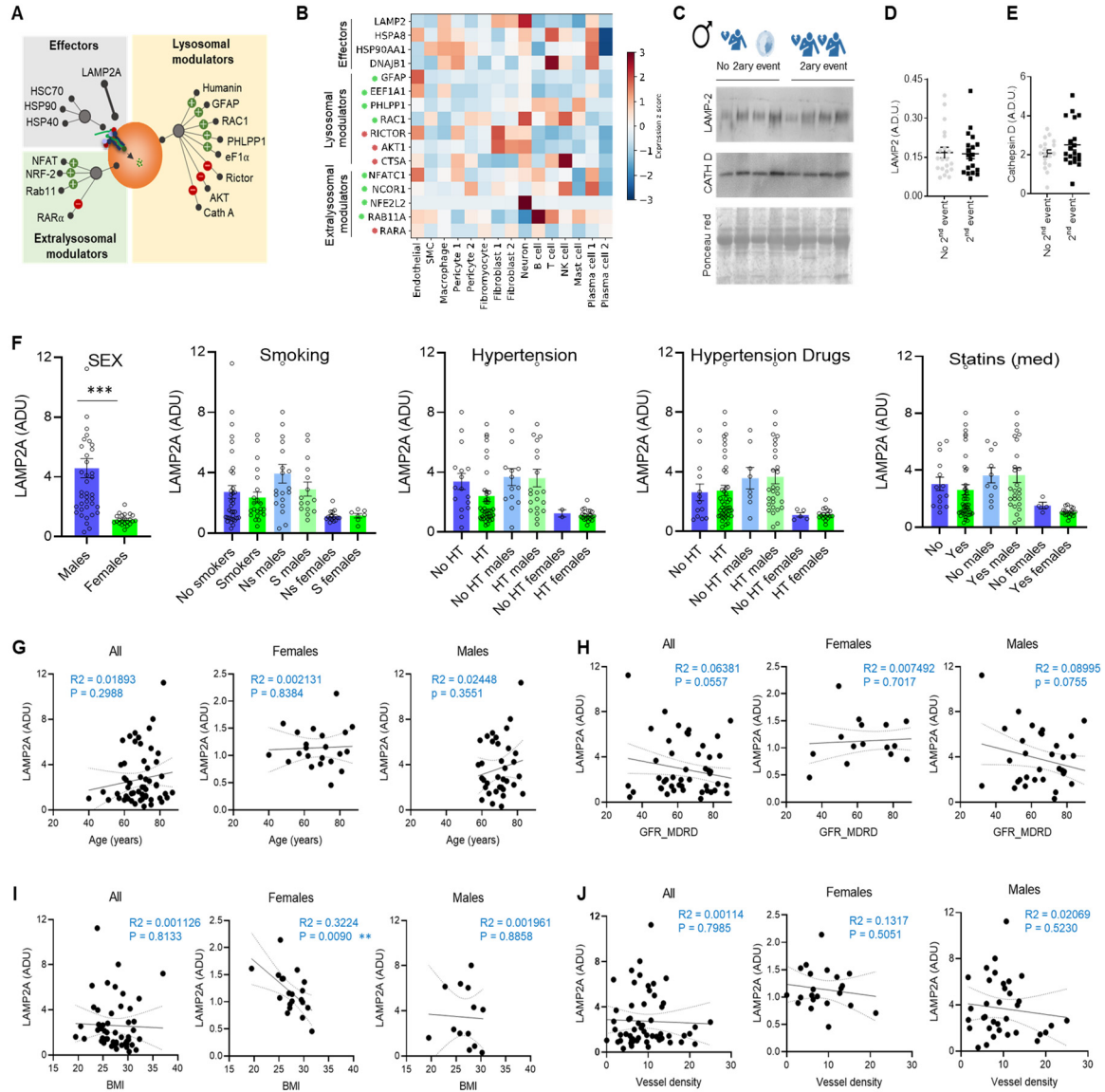


**Figure S6. Changes in CMA components in carotid from atherosclerosis patients.**

(A) Schematic representation of the CMA network. Proteins involved in CMA are grouped based on function (effectors and modulators) and localization (lysosomal and extra-lysosomal). (Diagram modified from (Kirchner et al., 2019)). (B) Normalized expression (within each cell type) of individual component of the CMA network in scRNAseq from atherosclerotic plaques. CMA network elements are organized in functional groups and colored dots indicate the effect of a given element on CMA activity (Green: positive element; Red: negative element). (C-E) Protein levels for LAMP2 and Cathepsin D in plaque lysates from male patients who underwent a secondary coronary event (2<sup>nd</sup> event) or not (no 2<sup>nd</sup> event) subjected to immunoblot. Representative immunoblot (C) and individual and mean values of the densitometric quantifications for LAMP2 (D) and cathepsin D (E) are shown as arbitrary densitometric units (A.D.U.). Ponceau red is shown as loading control. (F) L2A expression levels in subcategories of clinical parameters, stratified by sex. (G-J) Correlation scatterplots of L2A levels with age, BMI, glomerular filtration rate (GFR) as indication of diabetes and vessel density independent (all) or



stratified by sex. All data, when applicable, were tested for normal distribution using D'Agostino and Pearson normality test. Variables that did not pass normality test were subsequently analyzed using Mann–Whitney rank-sum test. All other variables were tested with the Student's t-test (D, E), one way ANOVA (F) or simple linear regression with  $R^2$  and p values indicated in blue (G-J). Individual patient values and mean  $\pm$  SEM (D-F) or linear regression (G-J) are shown. n=36.

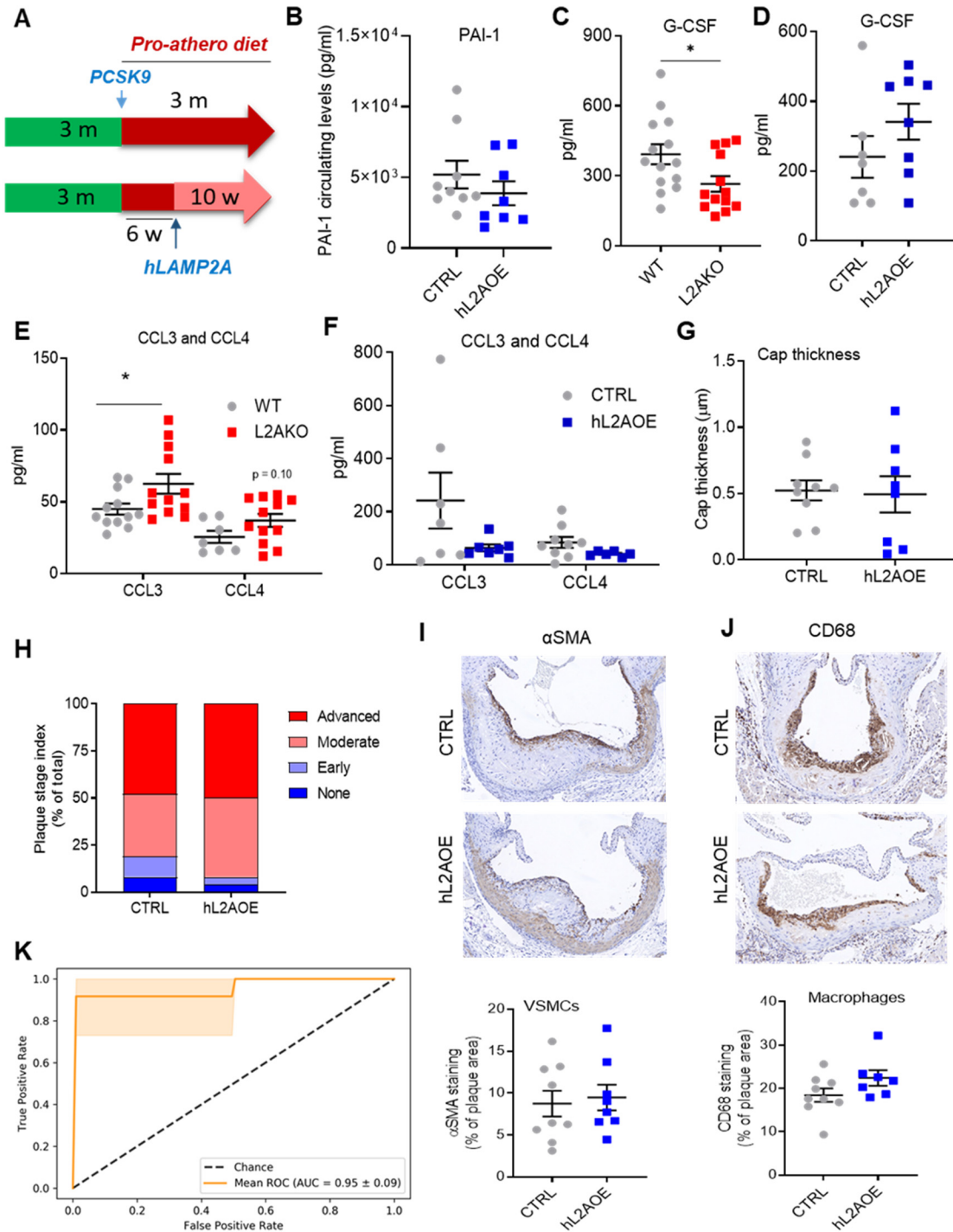


**Figure S7. Characterization of mice with genetic upregulation of CMA subjected to an experimental model of murine atherosclerosis.** (A) Scheme of the intervention to induce atherosclerosis (pro-athero) in mice systemically expressing a copy of human LAMP-2A (hL2AOE). (B-F) Levels of circulating PAI-1 (B), G-CSF (C,D) and CCL3 and CCL4 (E,F) in control (n=9) and hL2AOE (n=8) mice (B,D,F) and in wild-type mice (WT, n=15) and mice systemically null for LAMP-2A (L2AKO, n=16) (C,E). (G-J) Properties of the plaques from aortas of CTRL and hL2AOE mice subjected to the pro-atherosclerotic

intervention. Quantification of cap thickness (G), plaque stage (H) and representative images (top) and quantification (bottom) of aortas immunostained for  $\alpha$ SMA+ VSMC (I) and CD68 macrophages (J) Individual values (symbols) and mean  $\pm$  SEM are shown. n=9 CTRL, n=8 hL2AOE. (K) Receiver operating characteristic curve showing the performance of a support vector machine with linear kernel trained to classify animals between CTRL and hL2AOE groups. Orange line represents the mean performance over 5 folds cross validation. AUC: area under the curve, ROC: receiver operating characteristics. All data, when applicable, were tested for normal distribution using D'Agostino and Pearson normality test. Variables that did not pass normality test were subsequently analyzed using Mann-Whitney rank-sum test. All other variables were tested with the Student's t-test. Graphs represent mean  $\pm$  SEM. \*p <0.05.

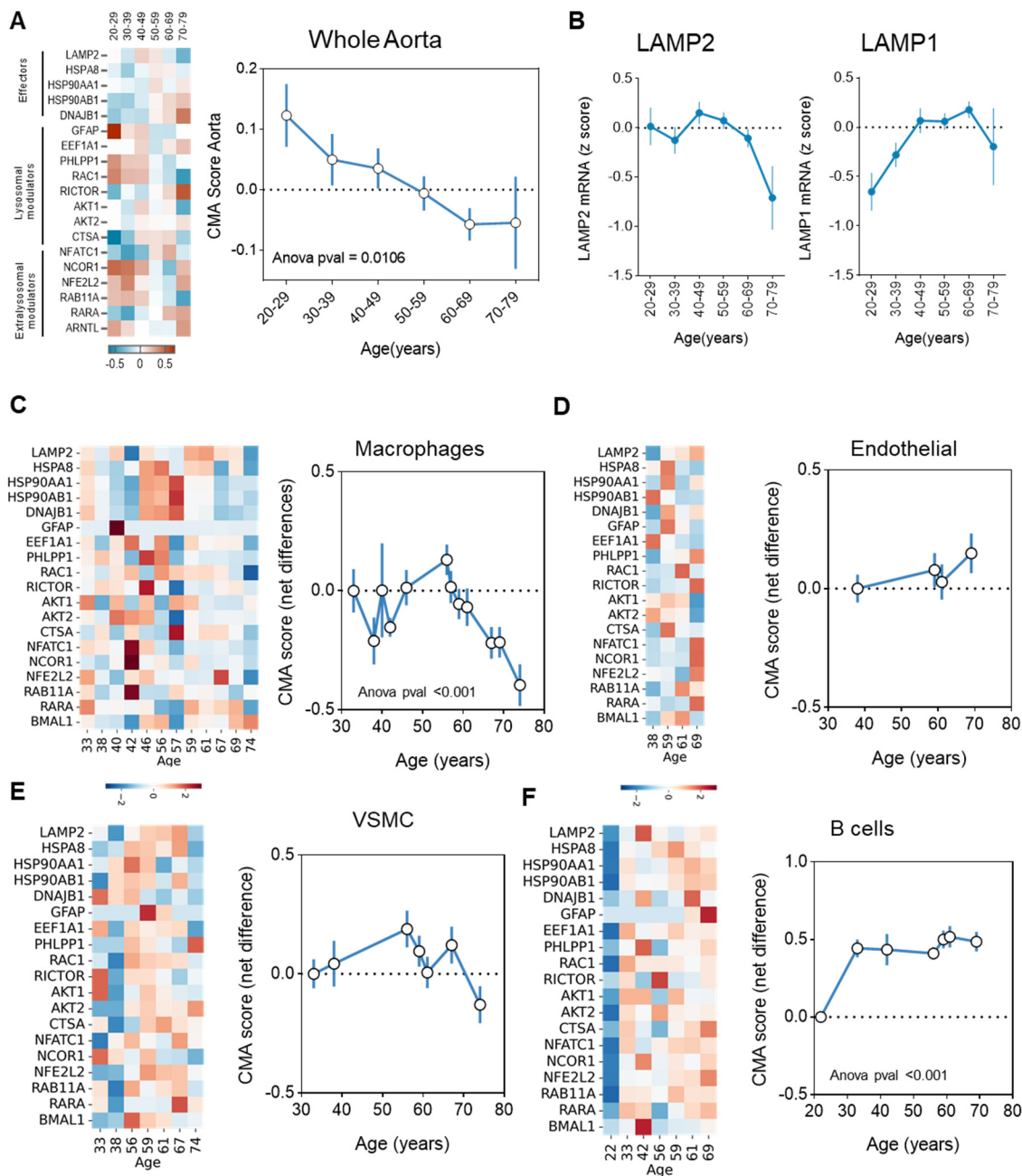


**Figure S8. Changes in CMA with age in human vasculature.** (A, B) Normalized expression of the CMA network components (left) and CMA activation score (right) (A) and LAMP2 and LAMP1 mRNA levels (B) in aorta from healthy individuals at the indicated ages calculated from RNAseq data in the GTEx aging database  $n = 432$  total samples (37, 38, 68, 149, 131 and 9 subjects for each age group shown, respectively). (C-F) Normalized expression of the CMA network components (left) and CMA activation score (right) expressed as net differences in the indicated cell types calculate from snRNAseq data in the Tabula Sapiens Consortium repository obtained from aortas of healthy subjects at the indicated ages.  $n = 5-13$ . Graphs represent mean  $\pm$  SEM. One-way ANOVA test was applied and p values are indicated in the graphs.

**Table S1. Blood leucocyte profile in CMA deficient mice in a Western-type diet.**

	WT	L2AKO	p-value
<b>CD45+ leucocytes</b>	9013 ± 378	9825 ± 620	ns
<b>B220+ B cells</b>	3825 ± 196	3273 ± 2931	ns
<b>NK.1.1+ NK cells</b>	193 ± 24	160 ± 10	ns
<b>NK.1.1 low CD3low NK T cells</b>	25.7 ± 3.9	21.5 ± 2.1	ns
<b>NK.1.1 low CD3low CD4+ NKT CD4 cells</b>	3.43 ± 0.68	2.91 ± 0.31	ns
<b>NK.1.1 low CD3low CD8+ NKT CD8 cells</b>	5.28 ± 0.78	5.84 ± 0.48	ns
<b>NK.1.1- CD3- Non NK T cells</b>	7250 ± 327	7596 ± 474	ns
<b>CD11B+ Ly6G+ Granulocytes</b>	1238 ± 84	1705 ± 113	***
<b>CD11B+ Ly6C- Monocytes</b>	1237 ± 107	1729 ± 144	*
<b>CD11B+ Ly6C- Low inflammatory monocytes</b>	680 ± 70	714 ± 61	ns
<b>CD11B+ Ly6C Med Monocytes mid-inflammatory</b>	152 ± 11	174 ± 15	ns
<b>CD11B+ Ly6C High inflammatory monocytes</b>	396 ± 40	832 ± 81	****
<b>CD3+ Total T cells</b>	1421 ± 75	1902 ± 145	**
<b>CD3+ CD4+ TCD4 cells</b>	707 ± 43	879 ± 55	*
<b>CD3+ CD8+ TCD8 cells</b>	617 ± 35	760 ± 46	*
<b>CD3+ CD8+ Ly6C high Tmem cells</b>	302 ± 22	336 ± 21	ns

Blood leukocyte count in wild type (WT) mice and mice systemically knocked out for LAMP-2A (L2AKO) maintained on a Western-type diet (n=15 per genotype). All data are expressed as counts/ $\mu$ l and were tested for normal distribution using D'Agostino and Pearson normality test. Variables that did not pass normality test were subsequently analyzed using Mann–Whitney rank-sum test. All other variables were tested with the Student's t-test. Graphs represent mean  $\pm$  SEM. \*p <0.05, \*\*p <0.01, \*\*\*p <0.005 and \*\*\*\*p <0.0001. ns = nonsignificant.

**Table S2. Sources of human data/samples utilized in this work**

STUDY		Source	Type of patient	Artery	Data	Ref.	Panel
ATHEROSCLEROSIS	1	Autopsy	Deceased, no cardiovascular symptoms	Carotid artery	Histology of different plaque types (n=6-9 per group). Anonymize data	This work	5A_D
	2	Surgery, CEA	Symptomatic patients	Carotid artery	Microarrays of paired, intraplaque comparison of plaque segments with and without IPH, with quantified plaque traits in adjacent histological segments (n=26 IPH, n=16 w.o. IPH)	Jin et al, 2021	5E, F, H,L
	3	Surgery, CEA	Symptomatic patients	Carotid artery	Prospective, 3-year follow-up study of recurring CV events with plaques collected at first event, and segmented for histology of plaque traits, and serial segments used for protein analysis.	Hellings et al, 2008	5K
	4	Heart transplants	Healthy donors, no cardiovascular symptoms	Coronary artery	Single cell sequencing of 4 human plaques. No histology	Wirka et al. 2019	5I+M

STUDY		Source	Type of patient	Sample	Data	Ref.	Panel
AGING	A1	GTEX portal	Healthy human subjects of different age groups	Aorta	RNAseq from artery aorta of individuals in the second (n=37), third (n=38), fourth (n=68), fifth (n=149), sixth (n=131) and seventh (n=9) decade of life.	Lonsdale et al. 2013	S8A, B
	A2	Tabula Sapiens	Normal human subjects (2 individuals with coronary artery disease were eliminated from the analysis)	Aorta	Single cells RNAseq of aorta (n=13, age range 22-79 years, 52% males). Specific donor characteristics in <a href="https://tabula-sapiens-portal.ds.czbiohub.org/wheretheadata">https://tabula-sapiens-portal.ds.czbiohub.org/wheretheadata</a>	Tabula Sapiens, 2021	S8C-F

**Table S3. Clinical - and plaque characteristics of the patients in study 4**

Characteristic	Single event (n=28)	Recurrent event (n=34)
Age (years, mean $\pm$ SD)	65,3 $\pm$ 1,8	72,3 $\pm$ 1,4*
Sex (% males)	60.7	67.6
Current or prior smoking (%)	38.5	38.2
Arterial hypertension (%)	59.3	84,8*
Body Mass Index	26,9 $\pm$ 0,5	27,4 $\pm$ 0,7
eGFR MDRD, (mL/min/1.73 cm <sup>2</sup> )	76,3 $\pm$ 3,1	66,2 $\pm$ 3,5*
Diabetes mellitus (%)	17.9	29.4
Medication lipid-lowering (%)	75	76.5
Medication anti-hypertensive (%)	71.4	85.3
Medication anti-platelet (%)	96.4	91.2
Medication anti-coagulant	7.1	17.6
PAOD history	35.7	32.4
Stroke history	14.3	26.5
CAD history	28.6	35.3
Stenosis contralateral (%)	29.6	53.1
Plaque phenotype		
Intraplaque hemorrhage (%)	71.4	79.4
Macrophage content (yes %)	53.6	52.9
smooth muscle content (yes %)	75.0	72.7
Collagen (yes %)	75.0	75.8
Calcification (yes %)	60.7	64.7
Lipid content (yes %)	85.7	73.5

\* P-value < 0.05 single vs. recurrent event, T-test for continuous variables, Fisher's exact test for binary variables mean  $\pm$ SEM. dGFR, estimated glomerular filtration rate; MDRD, Modification of Diet in Renal Disease. PAOD, Peripheral Arterial Occlusive Disease Clinical Presentation

**Table S4. Association of LAMP2A with risk of recurrent event at 3 year follow-up stratified for sex**

Gender	Parameter	B	S.E.	Wald	df	Sig.	Exp(B)
Female*	LAMP2A	-10,475	5,298	3,910	1	,048	,000
	Constant	10,877	5,550	3,841	1	,050	52942,6
Male**	Age	,29	,10	8,97	1	,003	1,3
	Hypertension	2,16	1,11	3,80	1	,051	8,7
	Constant	-21,04	6,98	9,09	1	,003	,000

Logistic regression analysis with forward, stepwise inclusion (wald) of square-root transformed L2A, age, hypertension and BMI stratified by gender (n=22 females, 37 males). \* -2 Log likelihood = 19,2; Cox & Snell R Square 0,31, Nagelkerke R Square 0,42; \*\* -2 Log likelihood = 26,9 ; Cox & Snell R Square 0,43, Nagelkerke R Square 0,56.



**Table S5 Cox regression analysis of L2A with time to recurrent event within 3 year follow-up stratified for sex**

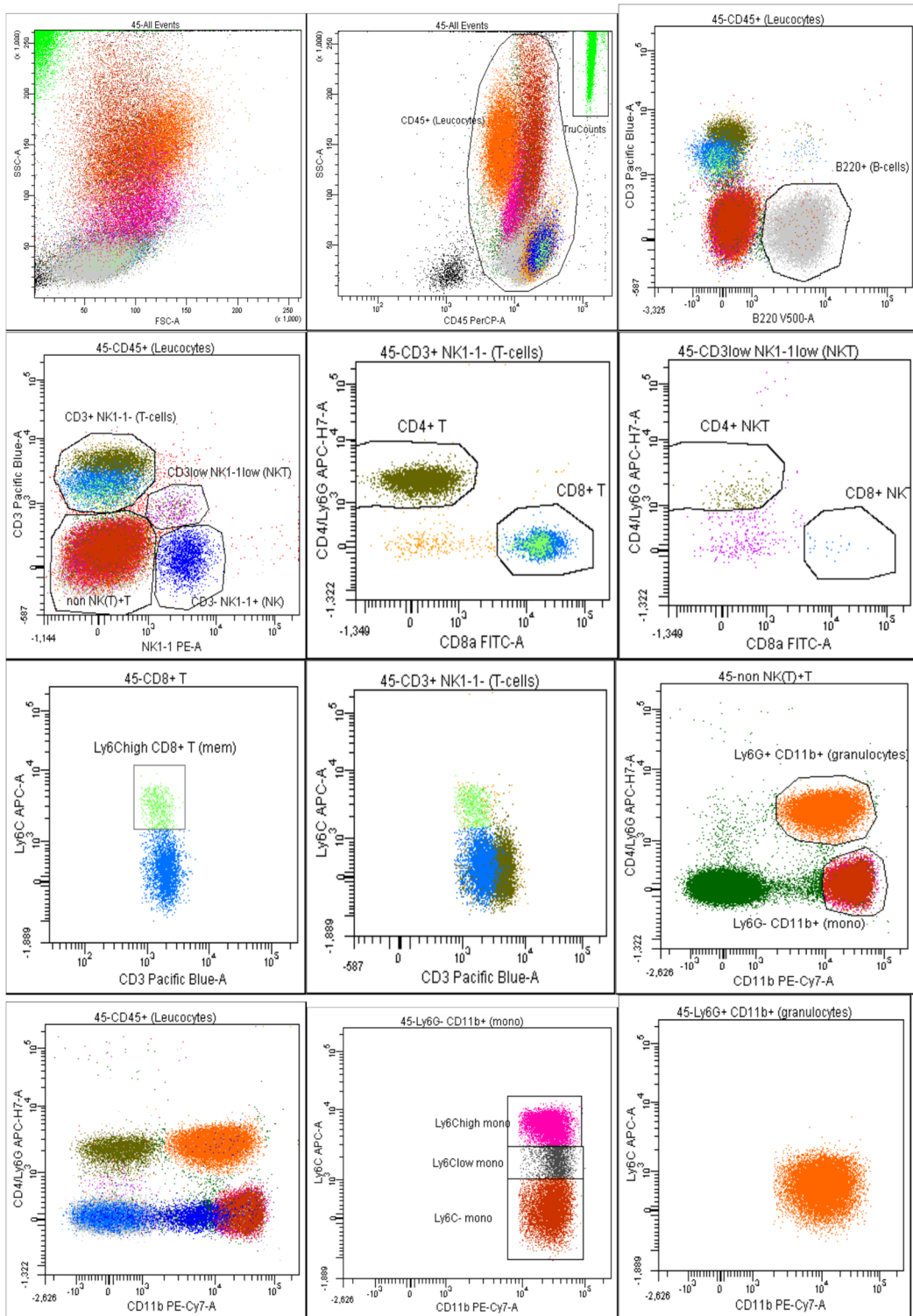
Gender	Parameter	B	S.E.	Wald	df	Sig.	Exp(B)
Female*	LAMP2A	-6,986	2,95	5,6	1	,018	,0
	Age	,001	,04	,0	1	,987	1,0
	Hypertension	13,024	814,98	,0	1	,987	453348,9
Male**	LAMP2A	-,007	,331	,000	1	,983	1,0
	Age	,154	,043	12,623	1	,000	1,2
	Hypertension	,532	,549	,938	1	,333	1,7

Cox regression analysis with time to recurrent event and square-root transformed L2A, age, and hypertension stratified by gender (n=22 females, 37 males). \* -2 Log likelihood = 37,43. \*\* -2 Log likelihood = 94,02.

**Table S6. List of primers for murine samples used in this study.**

<b>Gene</b>	<b>Forward primer</b>	<b>Reverse primer</b>
<b><i>Cd68 (tv 1)</i></b>	<i>GGACCGCTTATAGCCCAAGG</i>	<i>GGATGGCAGGAGAGTAACGG</i>
<b><i>Cdkn1a (tv 1)</i></b>	<i>CGGTGTCAGAGTCTAGGGGA</i>	<i>GCCTGTGGCTCTGAATGTCT</i>
<b><i>Cdkn1a (tv 2)</i></b>	<i>TGGAGACAGAGACCCCAGAT</i>	<i>CAGGATTGGACATGGTGCCT</i>
<b><i>Cdkn1b</i></b>	<i>CAGACGTAAACAGCTCCGAATTA</i>	<i>ACACAGGTAGTACAACAAAGCAA</i>
<b><i>Ptgs2 (Cox2)</i></b>	<i>CTTCGGGAGCACAACAGAGT</i>	<i>AAGTGGTAACCGCTCAGGTG</i>
<b><i>Lamp-2 (Lamp-2a, tv 1)</i></b>	<i>CTTAGCTTCTGGGATGCCCC</i>	<i>GCACTGCAGTCTTGAGCTGT</i>
<b><i>Nos2 (iNOS)</i></b>	<i>TCCTGGACATTACGACCCCT</i>	<i>AGGCCTCCAATCTCTGCCTA</i>
<b><i>Srebf2</i></b>	<i>GTCTCCCTGAGCTGGACCT</i>	<i>TAGCATCTCGTCGATGTCCC</i>

Tv: transcript variant.



Supplementary Scheme 1. Gating strategy for Fig. 4K-N and Supp. Table 1.

Source data. Uncropped immunoblots

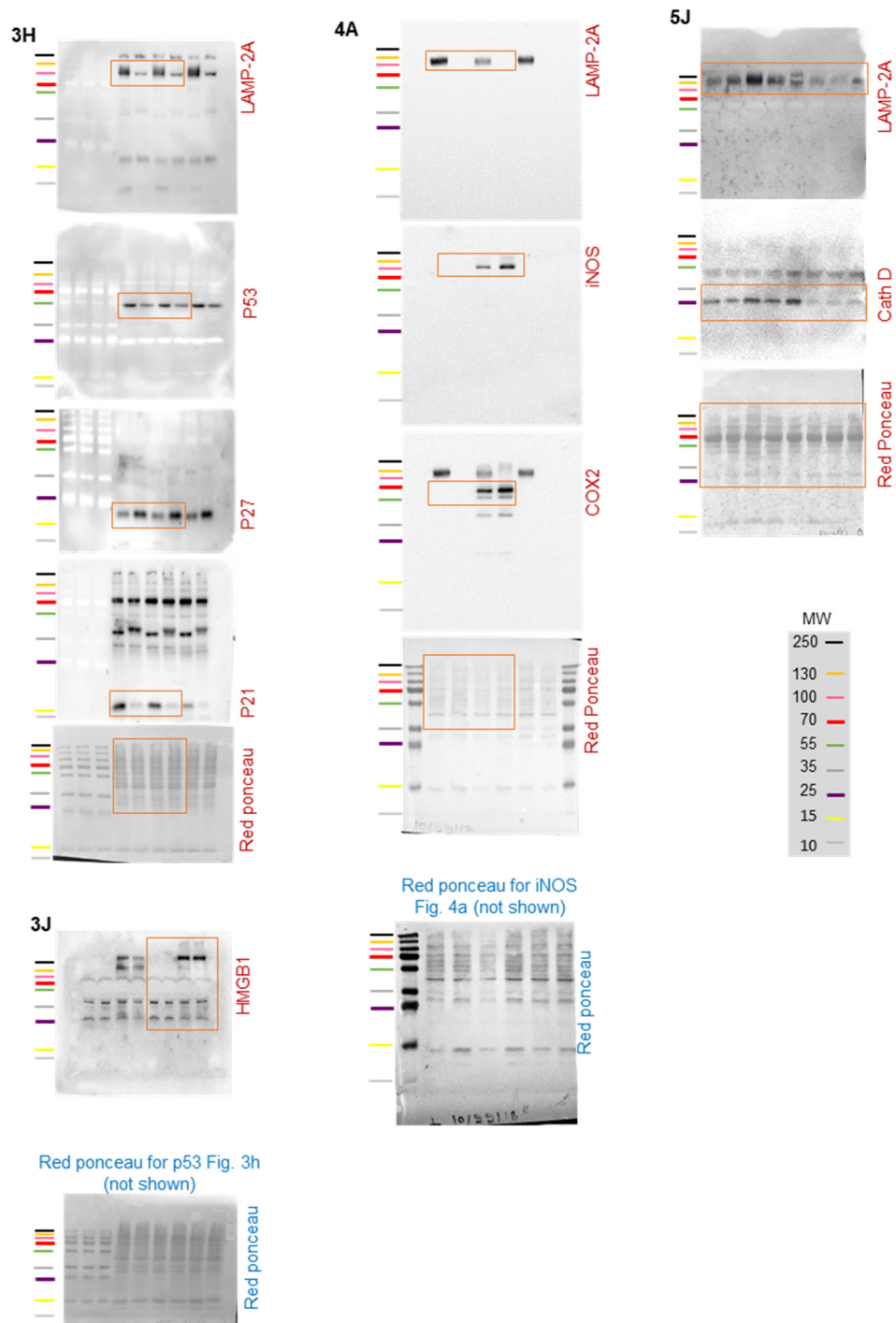


**Figure.** Merged images of uncropped immunoblots with molecular weight markers of the immunoblot data shown in the main figures. Molecular weight markers are color coded according to the key shown.

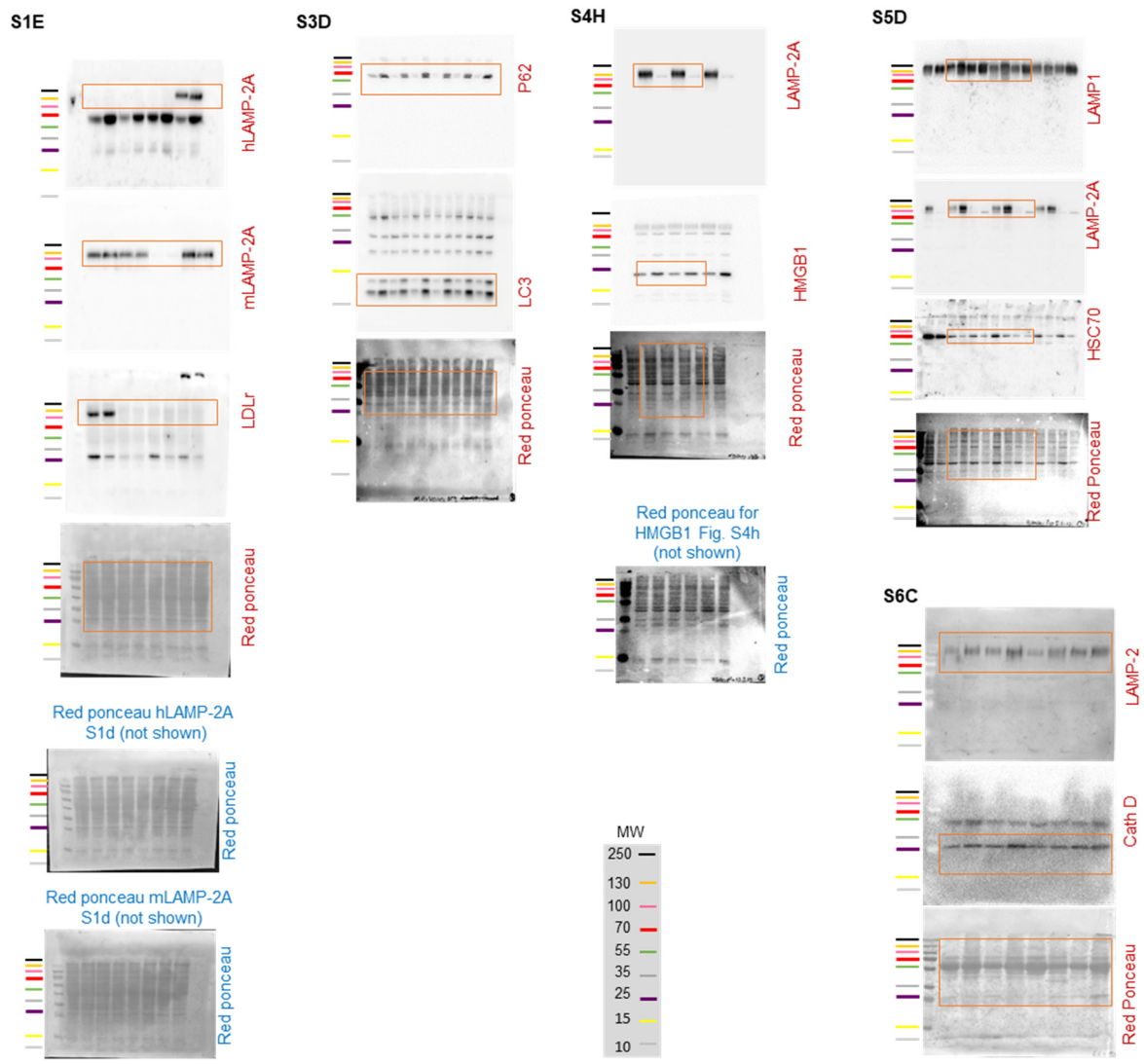


**Figure.** Merged images of uncropped immunoblots with molecular weight markers of the immunoblot data shown in the supplementary figures. Molecular weight markers are color coded according to the key shown.

**Dataset S1 (separate file).** Raw data and full statistical reports (Main and supplementary figures). See attached excel file

## SI References

1. S. Dong *et al.*, Monitoring spatio-temporal changes in chaperone-mediated autophagy *in vivo*. *Nat. Comm.* **15**, doi: 10.1186/s13024-13019-10354-13020 (2020).
2. J. L. Schneider, Y. Suh, A. M. Cuervo, Deficient chaperone-mediated autophagy in liver leads to metabolic dysregulation. *Cell Metab* **20**, 417-432 (2014).
3. S. Dong *et al.*, Chaperone-mediated autophagy sustains haematopoietic stem-cell function. *Nature* **591**, 117-123 (2021).
4. M. M. Bjorklund *et al.*, Induction of atherosclerosis in mice and hamsters without germline genetic engineering. *Circ Res* **114**, 1684-1689 (2014).
5. W. J. Huh *et al.*, Tamoxifen induces rapid, reversible atrophy, and metaplasia in mouse stomach. *Gastroenterology* **142**, 21-24 e27 (2012).
6. E. Araldi *et al.*, Lanosterol Modulates TLR4-Mediated Innate Immune Responses in Macrophages. *Cell Rep* **19**, 2743-2755 (2017).
7. C. A. Argmann *et al.*, Human smooth muscle cell subpopulations differentially accumulate cholesteryl ester when exposed to native and oxidized lipoproteins. *Arterioscler Thromb Vasc Biol* **24**, 1290-1296 (2004).
8. A. Canfran-Duque *et al.*, Macrophage deficiency of miR-21 promotes apoptosis, plaque necrosis, and vascular inflammation during atherogenesis. *EMBO Mol Med* **9**, 1244-1262 (2017).
9. F. O. Martinez, S. Gordon, M. Locati, A. Mantovani, Transcriptional profiling of the human monocyte-to-macrophage differentiation and polarization: new molecules and patterns of gene expression. *J Immunol* **177**, 7303-7311 (2006).
10. H. Jin *et al.*, Integrative multiomics analysis of human atherosclerosis reveals a serum response factor-driven network associated with intraplaque hemorrhage. *Clin Transl Med* **11**, e458 (2021).
11. R. Virmani, F. D. Kolodgie, A. P. Burke, A. Farb, S. M. Schwartz, Lessons from sudden coronary death: a comprehensive morphological classification scheme for atherosclerotic lesions. *Arterioscler Thromb Vasc Biol* **20**, 1262-1275 (2000).
12. R. C. Wirka *et al.*, Atheroprotective roles of smooth muscle cell phenotypic modulation and the TCF21 disease gene as revealed by single-cell analysis. *Nat Med* **25**, 1280+ (2019).
13. J. Lonsdale *et al.*, The Genotype-Tissue Expression (GTEx) project. *Nature Genetics* **45**, 580-585 (2013).
14. T. T. S. Consortium, S. R. Quake, The Tabula Sapiens: a multiple organ single cell transcriptomic atlas of humans. *bioRxiv* 10.1101/2021.07.19.452956, 2021.2007.2019.452956 (2021).
15. S. Kaushik, A. M. Cuervo, Degradation of lipid droplet-associated proteins by chaperone-mediated autophagy facilitates lipolysis. *Nature cell biology* **17**, 759-770 (2015).
16. E. Lutgens *et al.*, Deficient CD40-TRAF6 signaling in leukocytes prevents atherosclerosis by skewing the immune response toward an antiinflammatory profile. *J Exp Med* **207**, 391-404 (2010).

17. D. Olmeda *et al.*, Whole-body imaging of lymphovascular niches identifies pre-metastatic roles of midkine. *Nature* **546**, 676-680 (2017).
18. H. Koga, M. Martinez-Vicente, F. Macian, V. V. Verkhusha, A. M. Cuervo, A photoconvertible fluorescent reporter to track chaperone-mediated autophagy. *Nat Commun* **2**, 386 (2011).
19. E. Arias *et al.*, Lysosomal mTORC2/PHLPP1/Akt Regulate Chaperone-Mediated Autophagy. *Mol Cell* **59**, 270-284 (2015).
20. B. Storrie, E. A. Madden, Isolation of subcellular organelles. *Methods Enzymol* **182**, 203-225 (1990).
21. M. Bourdenx *et al.*, Chaperone-mediated autophagy prevents collapse of the neuronal metastable proteome. *Cell* **184**, 2696-2714 e2625 (2021).
22. P. Kirchner *et al.*, Proteome-wide analysis of chaperone-mediated autophagy targeting motifs. *PLoS Biol* **17**, e3000301 (2019).
23. J. Madrigal-Matute *et al.*, HSP90 inhibition by 17-DMAG attenuates oxidative stress in experimental atherosclerosis. *Cardiovasc Res* **95**, 116-123 (2012).
24. S. Kimura, T. Noda, T. Yoshimori, Dissection of the autophagosome maturation process by a novel reporter protein, tandem fluorescent-tagged LC3. *Autophagy* **3**, 452-460 (2007).